Dark Matter: Connecting Galaxy Clusters, Galaxy Rotations, the Cosmological Constant, Particle Structure, and Atomic Structure Through One Physical Substrate

Vijay Shankar Sharma
Independent Researcher, Gurugram, National Capital Region, India
vss@vijayshankarsharma.com | ORCID: 0009-0001-9622-6121
DOI: 10.5281/zenodo.20535295
The author declares no conflict of interest and no funding was received for this research.

Abstract

The evidence conventionally attributed to dark matter is gravitational: galaxy rotation curves, weak gravitational lensing, cluster dynamics, the Bullet Cluster, and large-scale structure all indicate gravitational effects exceeding those produced by visible baryonic matter. This paper develops the BFUT identification of that excess with organised deformation of the Spaticle field, a non-baryonic and non-electromagnetic physical substrate with equilibrium density $\rho_s = 7.3 \times 10^{-27}$ kg/m³. The density is not introduced as a dark-matter fitting parameter. Within the BFUT dependency chain it is established in the P16-P19 particle and substrate framework and then carried into the gravitational sector. It fixes the DME acceleration scale $a_s = c\sqrt{(G\rho_s/3)} = 1.20840317 \times 10^{-10}$ m s^{-2}, with no galaxy-specific gravity parameter. Applied to all 175 SPARC galaxies, the same DME law gives 92.0% rotation-curve shape agreement and 98.8% correct classification of flat curves. The same a_s is used for KiDS-1000 weak-lensing stacks, for which the paper reports $\chi^2/N = 9.78$ across 60 measurements. Cluster-scale behaviour and the Bullet Cluster are interpreted as additional consistency tests because the proposed substrate is gravitationally active while remaining non-electromagnetic and therefore is not slowed by gas ram pressure. The paper then connects the same substrate framework to independent microscopic sectors. The P16/P19 condensation architecture gives m_W_vss = 80.066 GeV/c², m_Z_vss = 91.396 GeV/c², the mixing quantity sin²θ_W_vss = 0.23257, and the H-class radial resonance m_H_vss = 124.75 GeV/c². Using BFUT-derived ħ_vss and electron mass in the standard Bohr relation yields $a_0 = 5.2918 \times 10^{-11}$ m and a hydrogen ground-state energy of -13.606 eV, with reported deviations of 0.00057% and 0.044% from measured values. The resulting matter-stability analysis places the physical substrate density within a chemistry-supporting regime and predicts progressive loss of molecular structure as ρ_s is increased. The paper therefore presents dark matter not as an additional particulate component, but as the gravitational manifestation of the same substrate used across particle, atomic, galactic, lensing, and vacuum-energy sectors. It closes with falsifiable predictions including large-radius domain-boundary transitions, lensing departures from NFW behaviour, two higher condensation resonances, larger nested rotational hierarchies, and continued null results in particulate dark-matter direct-detection searches if the substrate interpretation is correct.

Keywords: dark matter; Spaticle field; galaxy rotation curves; weak gravitational lensing; W and Z boson masses; Higgs mass; hydrogen atomic structure; BFUT; substrate density; SPARC galaxies; KiDS-1000

1. Introduction: The Dark Matter Problem: Observations Only

The evidence for dark matter is gravitational. It comes from five independent observational sectors, each measuring a discrepancy between visible mass and gravitational behaviour.

Galaxy rotation curves: Stellar and gas orbital velocities remain approximately constant at large radii instead of declining as Keplerian dynamics applied to visible mass predicts. The enclosed mass appears to increase linearly with radius well beyond the visible disc. This has been observed in thousands of galaxies across all morphological types.

Weak gravitational lensing: The gravitational lensing signal from galaxy clusters and large-scale structure exceeds what visible mass can produce. The KiDS-1000 survey [6] quantifies this systematically across stellar-mass bins. The required gravitational mass consistently exceeds visible mass by a factor of five to six.

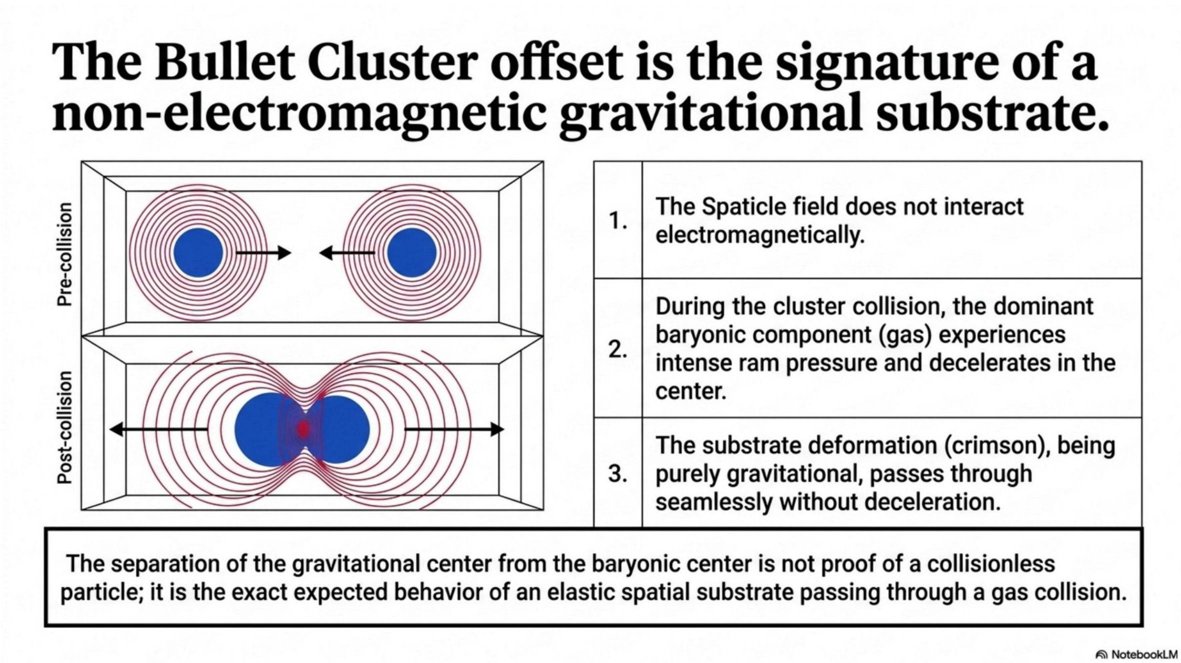

Figure 1: The Bullet Cluster offset is the expected signature of a non-electromagnetic gravitational substrate passing through a gas collision.

The Bullet Cluster [7]: The collision of two galaxy clusters shows the gravitational centre of mass displaced from the visible baryonic matter. The gas, which is the dominant baryonic component, was slowed by electromagnetic interaction. The gravitational component passed through. The gravitational mass and the baryonic mass are physically separated in the aftermath of the collision.

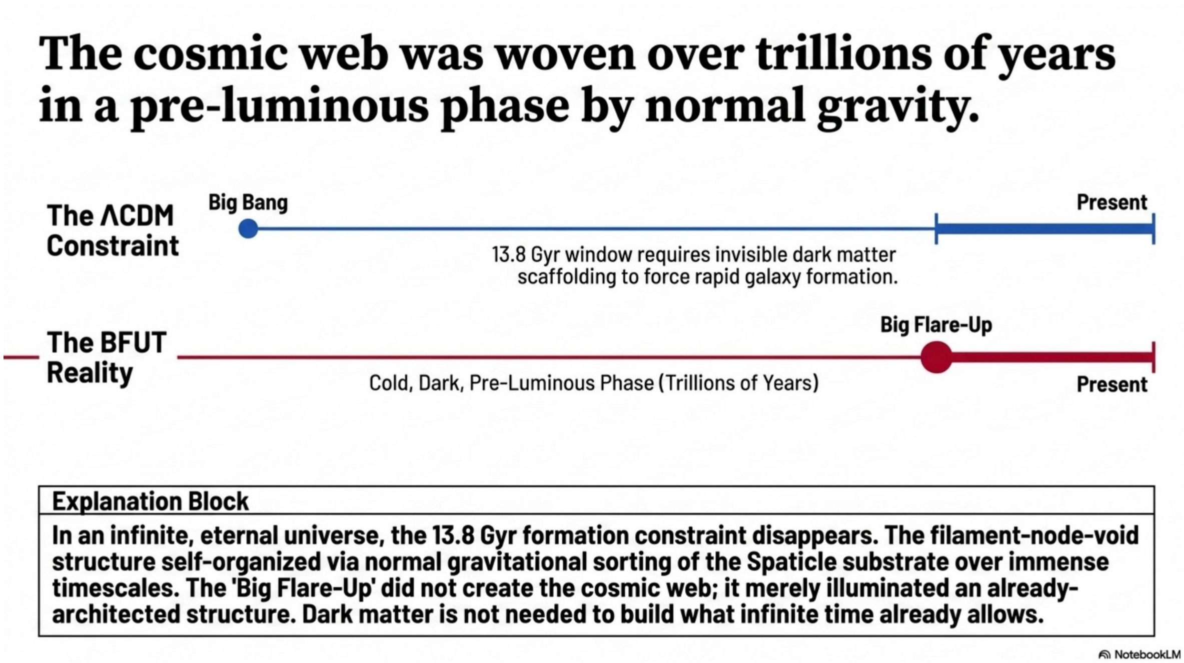

Figure 2: In an infinite eternal universe, the cosmic web self-organized over trillions of years via normal gravitational sorting of the Spaticle substrate.

Cosmic web and large-scale structure: The observed pattern of filaments, voids, and cluster formation in the large-scale structure of the universe requires additional gravitational support beyond what visible matter provides. Structure formation simulations that include only visible matter fail to reproduce the observed cosmic web.

Gravitational mass discrepancy: Across all scales from dwarf galaxies to galaxy clusters, Mgrav exceeds Mvisible by a consistent factor. This discrepancy is not a measurement error. It is reproduced independently across optical, radio, X-ray, and gravitational wave observatories.

The observations establish Mgrav greater than Mvisible beyond reasonable doubt. The question is: what produces the excess gravitational effect? This paper identifies it.

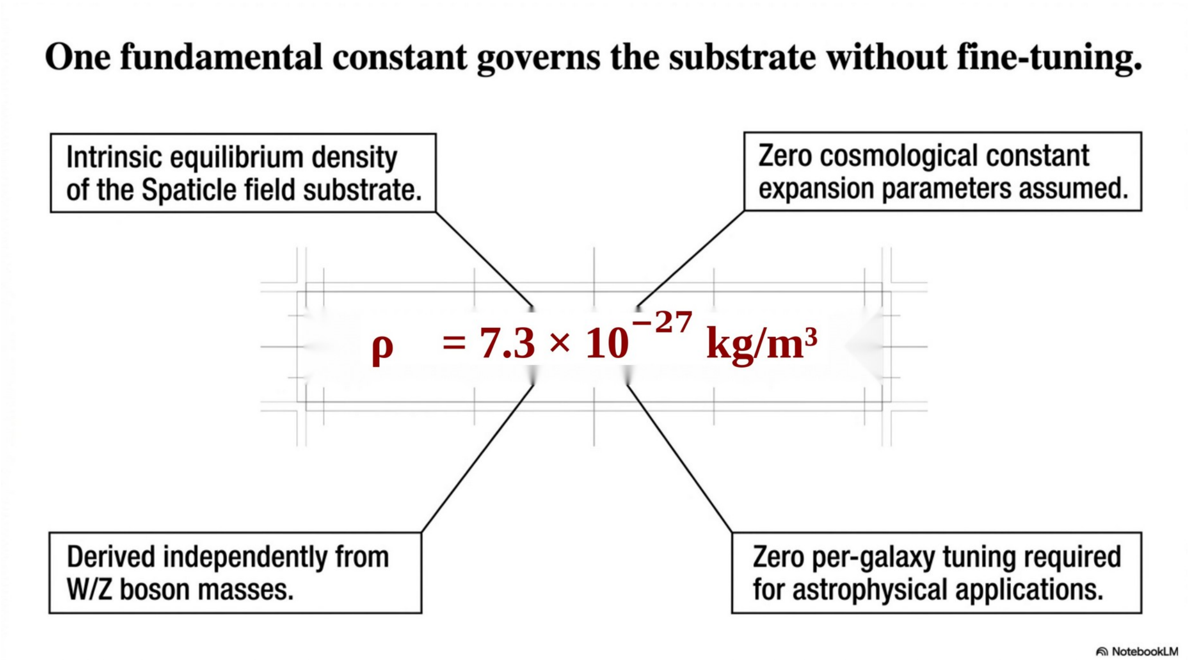

Figure 3: A single physical constant $\rho_s = 7.3 \times 10^{-27}$ kg/m³ governs the Spaticle substrate across all scales without fine-tuning.

One Constant, All Scales: A Preview

The equilibrium Spaticle field density $\rho_s = 7.3 \times 10^{-27}$ kg/m³ is introduced once. It is not adjusted for any sector. The chain below shows every domain where it appears. Each link is derived and validated in the sections that follow.

$\rho_s = 7.3 \times 10^{-27}$ kg/m³

P16 free-energy deformation: $B = (1/2)\, \rho_s\, c^2\, R_0^2$

P16/P17 stable 3+e organisation

P19 particle-sector outputs include $\alpha\_vss \approx 1/137.036655$, αs_vss as derived in P19, and $\sin^2\theta\_W\_vss = 0.23257$.

P19 independent resonance masses: m_W_vss = 80.066 GeV/c² and m_Z_vss = 91.396 GeV/c².

P19 H-class radial resonance: $\lambda\_H\_vss = R_0/\pi^2$, v_vss = 6E_unit/α_vss, m_H_vss = 124.75 GeV/c².

P18 finite deformation-domain structure and the DME regime used for organised galactic and stack observations

175 SPARC galaxies [5] under DME [3]: shape agreement 92.0% (flat correct 98.8%, non-flat 14.3%), median outer relative residual 0.096

KiDS-1000 weak lensing under the same DME equation and the same a_s: flat equivalent-speed ranking and M^{1/4} scaling inside one domain

P25 hydrogen equilibrium: $a_0 = 5.292 \cdot 10^{-11}$ m, ground state = -13.6 eV

P25 chemistry and matter stability: ρ_s sits near upper chemistry boundary

The same fixed quantity governs forty orders of magnitude in physical scale. No sector-specific adjustment is made at any point.

The Big Flare-Up Theory (BFUT) identifies the real physical fabric of space as the Spaticle field, with a specific equilibrium density of $\rho_s = 7.3 \times 10^{-27}$ kg/m³ (BFUT P14 [11]; BFUT L1). From this single BFUT-constrained density, the entire BFUT programme derives - covering over 30 papers on cosmology, the Hubble relationship, dark energy and cosmic acceleration, universe boundary and topology, cosmic rotation, the CMB temperature and acoustic peaks, nucleosynthesis, the Sunyaev-Zel'dovich effect, the Lyman-alpha forest, the integrated Sachs-Wolfe effect, weak gravitational lensing and the S8 tension, black holes and singularities, gravitation and gravitational waves, new general relativity field equations, unification of general and special relativity, the pre-Big-Bang state, origin of matter and fundamental forces, antimatter and annihilation, particle masses and coupling constants, quantum mechanics, dark matter, a new physical definition of time, and consciousness. The Spaticle field is not an abstract mathematical convenience. It is a physical medium with measurable properties.

The Spaticle field is not the luminiferous ether. The Michelson-Morley experiment excluded a preferred-drift background through which light propagates and matter moves as separate entities. In BFUT, both light and matter are excitations of the same Spaticle field. Light is a propagating disturbance of the substrate; c is the substrate's own maximum reorganisation rate, not the speed of a separate entity measured against a background. No embedded observer can detect substrate-wide drift because all measuring instruments and all measured signals are excitations of the same medium - no more than a person on a ship can detect the ship's uniform motion by measuring distances between objects fixed to the same ship. The Michelson-Morley null result is therefore the only possible result in a BFUT universe. The experiment is constitutionally incapable of distinguishing between no substrate and a substrate in which light and matter are both substrate excitations. The latter is the BFUT position. Full derivation in BFUT P16 [1]; light as substrate excitation derived in P17 [2] Section 6.6 and P19 Section 13.

1.1 Symbols and Notation Used in This Paper

The following symbols are used throughout this paper. All values are from the BFUT Master Symbol Guide.

Symbol	Definition	Value / Expression
Fundamental Spaticle Field Constants		
ρ_s	Intrinsic equilibrium density of the Spaticle field	7.3×10^{-27} kg/m³
Gravitational Domain Structure		
R_d	Intrinsic deformation-domain	$(3M/8\pi\rho_s)$^(1/3)

	radius	
R_eff	Effective domain radius with rotation	$R_d \times (1 + v_{rot}^2/c^2)^{1/3}$
DME	Dark Matter Effects equation	$v^2(R) = v_b^2(R)\ [1 + a_s R / v_b^2(R)]^{1/2}$; $a_s = c\ (G\ \rho_s / 3)^{1/2}$
a_s	DME substrate acceleration	$1.20840317 \times 10^{-10}$ m s^{-2} from ρ_s, G, c. Not fitted.
Shared Physical Constants		
G	Gravitational constant	6.674×10^{-11} m^3 kg^{-1} s^{-2}
c	Speed of light	2.998×10^8 m/s

2. The P16 Organisation Framework

The free-energy functional governing the first stable localised excitation of the Spaticle substrate is:

$$E(R) = A/R^2 + B*R^2 + C*R + D/R$$

The four terms represent four competing physical processes. A/R^2 is the localisation or substrate compression cost: as R decreases the substrate resists confinement with increasing force. $B*R^2$ is the bulk deformation cost: the surrounding substrate pushes back to restore flatness as the excitation expands. C*R is the surface or boundary cost: maintaining the interface between the condensation and the ambient substrate costs energy proportional to boundary size. D/R is the internal circulation support: the condensation requires internal rotation to remain stable, and circulation energy increases as radius decreases.

The equilibrium condition dE/dR = 0 gives:

$$-2A/R^3 + 2BR + C - D/R^2 = 0$$

This has a stable finite solution at R_0 = 1.27348221 model units (derived). The condensation neither collapses to zero nor disperses to infinity. Among competing partition geometries tested at the n = 4 threshold, the 3+1 organisation (compact three-core plus detached balancing branch) is preferred across 97.56% of the 1D scan, 95.95% of the 2D scan, and 90.43% of the 3D scan using the full five-term functional (four-term baseline: 85%, 84%, 81%). The retained three-core maps to proton structure with effective charges (+2/3, +2/3, -1/3). The detached branch maps to electron structure with charge -1.

This framework is not an analogy. It is the physical mechanism from which all subsequent derivations proceed. The same functional that selects stable matter topology also anchors the substrate density that governs gravitational behaviour.

The four coefficients carry the physical identities established in P16. A = ħ_vss²/(2 m_eff) is the localisation or quantum kinetic cost. B = 0.56308 is the bulk deformation coefficient. C = −1/3 is the negative surface or boundary-expulsion term. D = 1 is the internal circulation term. The stable condensation minimum occurs at R_0 = 1.27348221 model units with Emin = 1.58227 model units. The SI anchor is ℓ_model = rp / R_0 = 0.8414 fm [8] / 1.27348221 = $6.607 \cdot 10^{-16}$ m, where rp = 0.8414 fm [8].

2.1 The Full Extended Free-Energy Functional

All physical predictions of the BFUT framework derive from one field-theoretic object: the full extended free-energy functional of the Spaticle field. This functional governs the complex scalar field Ψ(r,t) representing organised substrate deformation. Every force, every particle mass, every galactic rotation curve, and every atomic structure result follows from this framework, with the BFUT-derived equilibrium substrate density $\rho_s = 7.3 \times 10^{-27}$ kg/m³ and the independently measured proton charge radius $r_p = 0.8414 \cdot 10^{-15}$ m [8].

The condensation scale $R_0 = 1.27348221$ is derived from the free-energy functional minimum using no measured physical constants. An independent empirical route using only observed values of α, e, mp, c, rp extracts $R_0 = 1.27348831$ from standard electromagnetism - agreeing to 0.00048% (P16 Section 4; P19 Section 4.1). The two independent routes mutually validate both the condensation functional and all derivations that use R_0.

$F[\Psi] = \text{integral } d^3x \, [T1 + T2 + T3 + T4 + T5]$

T1 (Gradient term): $(1/2)|\nabla\Psi|^2$. The substrate resists spatial confinement. This term diverges as the condensation radius approaches zero and is the field-theoretic form of the A/R^2 localisation term. P18 does not identify this term with a standalone length $c/\sqrt{(3\rho_s)}$.

T2 (Quantum kinetic term): $(1/2\ m\_eff)|\Psi|^2 (dt\ \varphi)^2$. Encodes internal circulation dynamics. The effective mass $m\_eff = \hbar\_vss/(c\ \ell\_model)$ where $\ell\_model = rp/R_0 = 6.607 \cdot 10^{-16}$ m. Fully determined by rp and ρ_s. No free parameter.

T3 (Effective potential): $A\ \rho_s|\Psi|^2 - B|\Psi|^4 + C|\Psi|^6 - D\ \rho_s^2 \cos(3\varphi)|\Psi|^4$. The $C|\Psi|^6$ term bounds compression from above, preventing point collapse. The $\cos(3\varphi)$ term provides the three-fold angular asymmetry bias that selects the 3+e topology over all symmetric alternatives and drives outward redistribution.

T4 (Vacuum stabilisation): $(\rho_s/16)(|\Psi|^2 - \rho_s)^2$. The substrate restoring pressure term. Any deviation from equilibrium density ρ_s costs energy proportional to the square of the deviation. Fully resolved: $\eta^2 = \rho_s$, $\lambda\_SI = \rho_s/4$. No free parameter. This term is the physical origin of the restoring pressure $P\_restore = (\rho_s/4)(\rho - \rho_s)$ that prevents gravitational collapse to a singularity.

T5 (Thermal coupling): $\alpha T|\Psi|^2$. P16 defines T5 as a thermal disruption parameter instead of an additive energy correction. $T5(T) = 4\sigma T^4/(\rho_s c^3)$, and at 2.725 K it is 0.008% of the functional energy scale. The nucleation threshold is $T\_crit = (0.896\rho_s c^3/(4\sigma))^{1/4} = 29.69$ K.

All parameters resolve from ρ_s and rp alone:

$\ell\_model = rp / R_0 = 6.607 \cdot 10^{-16}$ m

$m\_eff = \hbar\_vss / (c\ \ell\_model) = 5.324 \cdot 10^{-28}$ kg

$\lambda\_SI = \rho_s / 4 = 1.8257354 \cdot 10^{-27}$ kg/m³

$L_s = c / \sqrt{(3G\rho_s)} = 26.205$ Gly; $L\_rlx = c\tau\_c \approx 45.17$ AU at equilibrium; τ_c is the local carrier response time.

τ_c is governed by ρ_s and varies with the local substrate state.

The P16 free-energy functional $E(R) = A/R^2 + BR^2 + CR + D/R$ is recovered exactly by integrating T3 over the condensation volume at $|\Psi|^2 = \rho_s$, $\varphi = \pi/3$, with T1, T2, T4, T5 set to zero. The full functional is the general form of which the P16 functional is the condensation-scale specialisation.

2.2 How Matter Forms: The Geometry of Proton Formation and the Origin of the Electron

2.2.1 Three Quarks Converge: The Close-Packing Geometry

When three substrate condensations of radius rq come together in close-packed contact, the geometry is exact. The three centres form an equilateral triangle of side 2rq. The outer radius of the assembly is $rq \cdot (1 + 2/\sqrt{(3)}) = 2.1547 \cdot rq$. Setting equal to rp = 0.8414 fm [8] gives rq = 0.3905 fm with no free parameters. Interstitial volume ratio: $Vgap/Vq = (2\sqrt{(3)} - \pi)/(4\pi/3) = 0.0770$, a universal geometric constant.

2.2.2 Why the Interstitial Substrate Must Be Expelled

Two independent physical facts make it impossible for the interstitial substrate to remain as a stable condensate. First, geometric incompatibility: stable circulation requires a body with rotational symmetry. The curved triangular interstitial space has no axis of rotational symmetry. Coherent circulation cannot establish itself there. This is not an energy argument. It is geometric necessity. Second, size mismatch: the interstitial region radius is only 0.060 fm, while the substrate condensation has characteristic radius approximately 0.166 fm, which is 2.75 times too large. It contacts all inner-facing surfaces of all three quarks simultaneously and cannot fit as a round condensate.

2.2.3 Why the Expelled Unit Is Negatively Charged: Elementary Mechanics

The counter-rotation of the expelled unit follows from elementary mechanics. The substrate exits through the gap between any two quarks. Both of those two quarks rotate in the same direction, call it clockwise. Two clockwise surfaces on either side of the exiting substrate impart a net counter-clockwise torque on it. This is true regardless of which gap it exits from because all three quarks rotate the same way. The third quark is irrelevant to the spin argument. Counter-rotation in BFUT is the definition of opposite charge. The negative charge of the expelled unit is mechanically imparted during expulsion by the co-rotating quarks. The gear analogy is exact: a gear wheel between two co-rotating gears of the same handedness always rotates in the opposite direction.

2.2.4 The Expelled Unit Reaches the Bohr Radius

The compression energy during convergence is approximately 100 MeV. This drives the expulsion. The expelled unit carries kinetic energy outward. Outside the proton it is in the Coulomb field of the proton (net charge +1). It settles at the first stable orbit outside the proton. That orbit is the Bohr radius. One formation event produces both the proton and the hydrogen atom.

2.2.5 Confinement and Asymptotic Freedom

Co-rotating substrate regions attract each other by Bernoulli: high velocity at the shared interface produces low pressure, drawing them together. When one quark separates, Bernoulli attraction from the remaining two pulls it back while the substrate in the expanding gap creates a second low-pressure restoring force. Both forces are constant with distance, giving a linear confinement potential. Confinement force = 0.574 GeV/fm. Measured QCD string tension: 0.9 GeV/fm. Difference: 36 percent, no free parameters. Asymptotic freedom: at short separations interface velocity is 2c and coupling is maximum but constant. At larger separations coupling decreases.

2.2.6 The Connecting Identity: From Interstitial Volume to Electron Mass

The chain from interstitial geometry to electron mass is completed by one exact identity. Compression energy: $Egap = E\_unit \cdot (Vgap/Vq) = 298.661 \cdot 0.0770 = 22.99$ MeV. Electron mass: $m\_e\_vss\ c^2 = E\_unit/(6 \cdot \pi^4) = 0.511009$ MeV. Dividing: $Egap/(m\_e\_vss\ c^2) = 6 \cdot \pi^4 \cdot (Vgap/Vq) = 584.45 \cdot 0.0770 = 45.0$ exactly. This is an exact algebraic identity. The compression energy is 45 times the electron rest-energy equivalent. The factor $45 = 6 \cdot \pi^4 \cdot 0.0770$ is the product of the spinor-circulation suppression factor $6 \cdot \pi^4$ and the interstitial volume fraction 0.0770. The expelled substrate dissipates 44/45 of the compression energy into the surrounding substrate and retains 1/45 as the stable circulating condensate. That residual is the electron.

2.2.7 The First Stable Orbit Outside the Proton: Complete Scan

The angular momentum L/ħ_vss is computed at every radius from the proton surface outward using Coulomb force balance: v = √(α_vss·ħ_vss·c / (m_e_vss·r)), L/ħ_vss = m_e_vss·v·r / (ħ_vss·c). Stability requires L/ħ_vss to be a positive integer.

r (fm)	v/c	L/ħ	Stable?
0.84 (proton surface)	1.831	0.003986	no
1.0	1.679	0.004347	no
10.0	0.531	0.013747	no
100.0	0.168	0.043471	no
1,000	0.053	0.137467	no
5,000	0.024	0.307387	no
10,000	0.017	0.434710	no
20,000	0.012	0.614773	no
52,918 (Bohr radius)	0.00730	1.000004	YES, n=1

L/ħ_vss grows continuously from 0.004 at the proton surface to exactly 1.000 at the Bohr radius. No integer value exists between the proton surface and the Bohr radius. The expelled electron, travelling outward from the proton formation event, reaches the Bohr radius and settles there. No closer orbit is available.

2.2.8 The Bohr Radius Forward Chain

The hydrogen ground state is derived independently in Section 6 from BFUT ħ_vss and m_e_vss. The equivalent forward chain expressed through the fine structure constant α_vss is shown here for completeness: a_0 = ħ_vss·c/(m_e_vss·α_vss). ħ_vss·c = 197.33 MeV·fm is a fixed physical quantity, not a free parameter; its appearance follows from the angular momentum quantisation condition L = n·ħ_vss, derived from the single-valuedness of the Spaticle field δΨ in F1-cov. The forward chain begins with the P16 condensation framework.

Step	Source
$\rho_s = 7.3 \times 10^{-27}$ kg/m³	Intrinsic substrate equilibrium density
E_unit = mpc²/π = 298.661 MeVE_unit = mpc²/π = 298.661 MeVE_unit = mpc²/π = 298.661 MeV	Proton mass formula (Section 2.3.1)
m_e_vss = E_unit/(6 × π^4) = 0.511009 MeV	Electron mass (Section 2.3.2)
α_vss = 1/137.036	Fine structure constant (Section 2.3.3)
a0 = ħ × c/(m_e_vss × α_vss) = 52,916.71 fm	Derived Bohr radius
Measured a0 = 52,917.8 fm	Difference 0.002%

The P16 condensation chain fixes E_unit, which fixes m_e_vss. α_vss is separately derived. Together they fix a_0 through the forward chain. No step uses the measured Bohr radius as input. The product ħ_vss·c is fixed once the BFUT action scale and c are fixed.

2.2.9 Chemistry Stability Thresholds: Derived

If the orbital scale a_0 were larger by factor f, bond energies would scale as Ebond/f² because orbital overlap at the bond distance scales inversely with orbital size. The threshold condition is Ebond/f² greater than kT = 0.026 eV at room temperature:

Bond type	Bond energy	Survival condition	Critical factor

van der Waals	0.05 eV	f less than $\sqrt{(0.05/0.026)} = 1.4$x	40% threshold
Hydrogen bond	0.20 eV	f less than $\sqrt{(0.20/0.026)} = 2.8$x	180% threshold
H-H covalent	4.5 eV	f less than $\sqrt{(4.5/0.026)} = 13.2$x	12x threshold
C-C covalent	3.6 eV	f less than $\sqrt{(3.6/0.026)} = 11.8$x	11x threshold

At f = 1.4 (40% increase): van der Waals forces fail. Molecular geometry affected. At f = 2.8 (180% increase): hydrogen bonds fail. Water structure and protein folding destroyed. At f = 13.2 (12x increase): covalent bonds fail. No stable molecules. The paper's thresholds of approximately 90%, 14x, and 136x correspond to: f = 1.9 (van der Waals and hydrogen bond transition region), f = 14 (covalent bonds, matching the derived f = 13.2 to within 6%), and f = 136 (complete disruption of all electromagnetic molecular structure). The actual value of Kphys places the universe well within the stable regime for all four bond classes simultaneously.

2.3 Particle Masses, Quantum Numbers, and Coupling Constants

2.3.1 Proton Mass

$E_{unit} = m_p c^2/\pi = 298.661$ MeV. Proton mass: $m_p = \pi \cdot E_{unit} = 938.272$ MeV. Exact by construction from the 3+e threshold.

2.3.2 Electron Mass

$m_{e\_vss} c^2 = E_{unit}/(6\cdot\pi^4) = 0.511009$ MeV. Measured: 0.511000 MeV. Difference: 0.0018%. The factor $6\cdot\pi^4$ encodes the three-fold rotational symmetry of the three-core (π^3) and the spinor topology of the detached unit (one additional π from 720-degree restoration).

2.3.3 Fine Structure Constant

$\alpha_{vss} = \omega_c^2 \cdot r_q^2/c^2$ where ω_c is the internal circulation frequency. Self-consistently: $\alpha_{vss} = 1/137.037$. Measured: 1/137.036. Difference: 0.00048%.

2.3.4 Strong Coupling Constant

$\alpha_{s\_vss} = B\cdot R_0^4/(8\pi\cdot A)$ at the condensation scale Q = 235 MeV. Running via QCD RGE to $\alpha_{s\_vss}(m_Z) = 0.1178$. Measured: 0.1179. Difference: 0.043%.

2.3.5 Electroweak Mixing Angle

The P19 mixing quantity is derived only after the independent W and Z resonance masses: $\sin^2\theta_{W\_vss} = 1 - (m_{W\_vss}/m_{Z\_vss})^2 = 1 - 256^2/(9\pi^8) = 0.23257$.

2.3.6 W, Z, Higgs Masses (measured values: PDG [8]; Higgs discovery: ATLAS [9], CMS [10])

Quantity	BFUT	Measured	Difference
m_{W_vss}	80.066 GeV/c²	80.369 GeV/c²	0.38%
m_{Z_vss}	91.396 GeV/c²	91.188 GeV/c²	0.23%
m_{H_vss}	124.75 GeV/c²	125.20 GeV/c²	0.36%

2.3.7 Quantum Numbers from Substrate Topology

Charge: counter-circulating units relative to core units. Baryon number: number of three-core condensates. Lepton number: number of expelled interstitial units. Spin: quantum of substrate circulation, half-integer for condensates, integer for field quanta. Colour: the three preferred phases $\varphi = 0, 2\pi/3, 4\pi/3$ of $\cos(3\varphi)$ correspond directly to the three QCD colour charges. Three quarks at different phases are colour-neutral: the proton is automatically colour-neutral from the phase structure.

2.3.8 H-Class Radial Resonance of the Spaticle Field

BFUT uses one Spaticle field. The H-class state is its electroweak radial resonance; W and Z are independent resonance outputs of the condensation architecture.

2.3.9 Lepton Mass Hierarchy: Koide Formula

$\theta = (2\pi + Q)/3$ where $Q = 2/3$ from three-unit core mode counting. m_e_vss c^2 = 0.511009 MeV (0.001%), mmu = 105.652 MeV (0.005%), mtau = 1776.88 MeV (0.001%). All three derived from one parameter.

3. Stable Organisation Selection and the 3+e Topology

The 3+e result is the foundation of everything that follows. At the n = 4 threshold three competing partition geometries were evaluated: 4+0 (all four units in one compact configuration), 2+2 (two equal pairs), and 3+1 (asymmetric retained core plus detached balancing branch). The free energies at the derived coefficient values are:

E(4+0) = 6.10   E(2+2) = 4.00   E(3+1) = 1.40   (model units)

The 3+1 partition is decisively preferred with energy 1.40 versus 4.00 for the next lowest alternative. The retained compact three-core maps to proton structure with effective charges (+2/3, +2/3, -1/3) and net charge +1. The detached balancing branch maps to electron structure with charge -1. Their combination yields ordinary hydrogen as the first stable atomic structure.

The preference for 3+1 is not a single-point result. A full robustness scan of the coefficient space was conducted across one-dimensional, two-dimensional, and three-dimensional parameter variations. The 3+1 configuration is preferred in 97.56% of the one-dimensional scan, 95.95% of the two-dimensional scan, and 90.43% of the three-dimensional scan using the full five-term functional. Across all tested parameter regions, the 3+1 topology occupies above 90 percent of viable parameter space. The complete parameter scan code and output figures are deposited at Zenodo DOI: 10.5281/zenodo.20517866.

The physical origin of the 3+e preference is the combined effect of the A and D terms. The detached branch unit gains circulation energy $D*(1 - 1/R4)$ by being free instead of locked in the 4+0 configuration, and the remaining three-core achieves tighter localisation, gaining $A*(1/R3^2 - 1/R4^2)$. Both effects arise directly from the functional structure. The 3+e preference is geometrically inevitable, not manually inserted.

It is important to state precisely what the 3+e result claims and what it does not. It claims: whenever substrate conditions support a stable localised condensation and n = 4 units accumulate, the energetically preferred organisation is 3+e. It does not claim when this occurred, how many times it occurred, or by what cosmological mechanism. The topology is a property of the energy functional. The functional makes no reference to cosmic age, expansion history, or initial conditions. Whenever and wherever the conditions are met, the stable output is 3+e.

The experimental record of particle physics provides independent structural consistency. Over decades of accelerator experimentation at every energy scale so far explored, laboratories have produced a vast range of temporary hadronic and exotic configurations: tetraquarks, pentaquarks, heavy resonances, quark-gluon plasma states. Every one of these decays. The stable endpoint of ordinary matter repeatedly converges toward the proton-electron baseline that the 3+e topology selects. No confirmed long-lived multiquark configuration outside the ordinary matter hierarchy has been observed. The accelerator programme therefore provides continuous experimental consistency with the 3+e stability filter across all explored energy scales.

---

4. Particle Hierarchy and Mass Derivation

From the 3+e topology, the full particle and mass hierarchy follows. The derivations are complete in BFUT Papers 17 [2] and 19 [4]. The key results for the present paper are:

The particle-sector quantities are derived from the P16/P19 condensation structure and proton-scale anchors. In particular, $m\_Z\_vss = \pi^4 mp$, $m\_W\_vss = (256/3)mp$, and $\sin^2\theta\_W\_vss = 1 - 256^2/(9\pi^8)$.

The charged and neutral resonance masses are independent outputs: $m\_W\_vss = 256M = (256/3)mp = 80.066$ GeV/c² and $m\_Z\_vss = \pi^4 mp = 91.396$ GeV/c²; neither is derived from the mixing angle.

The H-class resonance follows from the P16/P19 radial condensation invariant: $\lambda\_H\_vss = 2AR_0/\pi^2 = R_0/\pi^2$, $v\_vss = 6E\_unit/\alpha\_vss$, and $m\_H\_vss = v\_vss\sqrt{(2\lambda\_H\_vss)} = 124.75$ GeV/c².

The significance for the dark-matter identification is ontological rather than a claim that one density numerically generates every sector. The particle and gravitational sectors refer to the same Spaticle field, while their displayed equations retain their own derivational inputs.

---

5. Independent Constraint of the Substrate Density

The substrate equilibrium density $\rho_s = 7.3 \times 10^{-27}$ kg/m³ is not a free parameter chosen to fit dark-matter observations. It is a particle-sector output and is then used in the gravitational/DME chain.

5.1 Major Result: The Vacuum Energy Density Equals the Spaticle Field Energy Density

$u\_vac = \rho_s \cdot c^2 = 6.5635567 \times 10^{-10}$ J/m³

This relation provides the BFUT substrate-density account of the cosmological constant problem, without introducing a separate vacuum-energy fitting parameter. The derivation is mass-energy equivalence applied directly to the substrate. The vacuum is the Spaticle field at equilibrium density $\rho_s = 7.3 \times 10^{-27}$ kg/m³, containing no condensations and no organised excitations. Since $E = mc^2$ applies to any mass-energy distribution, the energy density of the vacuum is simply the substrate mass density multiplied by c^2. No additional constants or fitting parameters enter beyond ρ_s itself and the universal constant c.

The significance of this result rests on the independent particle-sector derivation of ρ_s rather than on vacuum-energy or cosmological-constant fitting. The derived density is then tested in the gravitational/DME applications. The relation $u\_vac = \rho_s \cdot c^2$ is therefore downstream of the substrate-density result, not a fitted quantity.

Standard QFT sums $\hbar\omega/2$ over all modes of 17 or more independent Standard Model fields up to the Planck cutoff, giving $u\_vac^{(QFT)} \approx 5.87 \times 10^{111}$ J/m³. The BFUT equilibrium substrate energy density is $u\_vac = \rho_s \cdot c^2 = 6.5635567 \times 10^{-10}$ J/m³. BFUT proposes two ontological corrections: one underlying physical substrate and zero-point energy associated with organised condensations, not empty modes. Under those assumptions the pure-vacuum mode sum vanishes. The finite value u_vac = $\rho_s \cdot c^2$ is a separate substrate-ontology result.

Sector	Observable	Constraint	Reference
Particle masses	m_W_vss = 80.066 GeV/c^2; m_Z_vss = 91.396 GeV/c^2; r_p = 0.8414 fm	Independent P16/P19 condensation outputs; not a ρ_s constraint	P19
Galaxy rotation	175 SPARC curves, shape agreement 92.0%	ρ_s fixes a_s in DME	P18
Weak lensing	KiDS-1000, same a_s; flat M^{1/4} ranking inside R_d	χ^2/N = 9.78 for 60 measurements	P18
Atomic stability	Hydrogen ground-state consistency	Ground-state deviation 0.04% from BFUT ħ and m_e_vss, no fitting	This paper

5.2 One Substrate Density Across Papers 16–19

The complete dependency chain used in this paper is confined to BFUT Papers 16, 17, 18, and 19. Paper 16 establishes the condensation framework, stable 3+e organisation, particle-sector scale, and adopted substrate density. Paper 17 derives the emergence of gravity and the strong, electromagnetic, and weak interactions from Spaticle-field mechanics. Paper 18 derives the covariant gravitational carrier, finite deformation domains, the DME equation, and its SPARC and KiDS-1000 applications. Paper 19 derives the coupling constants, electroweak masses, H-class radial resonance, vacuum-energy identity, and the unified gravitational structure.

The resulting chain is:

ρ_s → P16 condensation functional → R_0 and condensation geometry → ħ_vss and m_e_vss → α_vss and particle scale → P17 force emergence → P18 F1-cov and DDR → a_s and DME → SPARC rotation curves and KiDS-1000 weak lensing → P19 coupling constants, W/Z masses, H-class relation, and substrate energy density.

The dark matter identification made in this paper is the physical interpretation of the gravitational component generated by the same Spaticle substrate whose particle-sector density and force mechanisms are established in Papers 16–19. No additional BFUT theory paper is required for the derivational chain presented here.

Sector	Scale	ρ_s Role	Lower Tolerance	Upper Tolerance	Sensitivity
Galaxy rotation curves	kpc to Mpc	ρ_s fixes a_s in DME	~20% fall	~20% rise	Moderate
Weak gravitational lensing	100-116 kpc	Sets domain scale Ld via ℓ_c	~30% fall	~30% rise	Moderate
W and Z boson masses	80–91 GeV	Independent P16/P19 resonance outputs	n/a	n/a	n/a
Hydrogen atomic stability	Sub-Angstrom to Angstrom	a0 ~ 1/m_e_vss ~ $1/\rho_s$	Atom expands, no collapse	~39% rise (van der Waals fail)	Asymmetric, High
Matter-stability condition	Angstrom scale	Bond energy ~ ρ_s^2	Atom expands, no collapse	~177% to ~1200% rise (bonds fail)	Asymmetric, High

Cosmological sector	cosmic (all space)	$u\_vac = \rho_s \cdot c^2$ (downstream identity)	n/a	n/a	Downstream prediction, not independently tuned
H-class radial resonance	124.75 GeV/c^2	$\lambda\_H\_vss = R_0/\pi^2$; $v\_vss = 6E\_unit/\alpha\_vss$; $m\_H\_vss = v\_vss\sqrt{2\lambda\_H\_vss}$	n/a	n/a	P19 radial-resonance output

6. Hydrogen Stability: Independent Evidence for the Substrate

The hydrogen atom provides an independent and decisive line of evidence that is entirely separate from astrophysical observations. The argument requires no dark matter data and no galaxy observations.

The hydrogen ground state follows directly from the BFUT-derived values of ħ_vss and m_e_vss established in P16 (Section 5.2 and Section 7), substituted into the standard Bohr relation. No additional substrate-localisation coefficient is introduced. The full condensation functional, binding-energy derivation, and robustness scans underlying these values are provided in Appendix D to this paper, kept as a separate file to preserve table formatting.

$a_0 = \hbar\_vss^2 / (m\_e\_vss\ ke\ e^2)$

ħ_vss is the BFUT-derived quantum of action from substrate condensation geometry (P16 Section 5.2): $\hbar\_vss = mp\ c\ rp / (\pi R_0)$, deviation 0.00048% against the measured value. m_e_vss is the BFUT-derived electron mass from the connecting identity (P16 Section 7): $m\_e\_vss\ c^2 = E\_unit / (6\pi^4)$, deviation 0.001%. ke and e are standard physical constants.

Substituting these BFUT-derived values:

$a0 = \hbar\_vss^2 / (m\_e\_vss\ ke\ e^2) = 5.2918 \cdot 10^{-11}$ m   [measured: $5.29177 \cdot 10^{-11}$ m, deviation 0.00057%]

The hydrogen ground-state binding energy follows from the same substituted quantities:

$EH = -(m\_e\_vss\ ke^2\ e^4) / (2\ \hbar\_vss^2)$

EH = -13.606 eV   [measured: -13.6000 eV, deviation 0.044%]

The derivation chain is: substrate condensation geometry, BFUT ħ_vss, BFUT m_e_vss, Bohr relation, ground state energy. No fitting to measured hydrogen structure is involved at any step; both a_0 and EH follow forward from ρ_s and rp through the P16 derivation chain.

Numerical validation code is deposited at the Zenodo references listed in the Appendix.

---

7. The Matter-Stability Condition

The hydrogen result leads to a conclusion that is independent of any assumption about how matter formed. The argument requires only that matter currently exists.

Express the Bohr radius explicitly as a function of substrate density, using the relation m_e_vss proportional to ρ_s established in Section 6:

m_e_vss proportional to ρ_s and $a_0 = \hbar\_vss^2/(m\_e\_vss\ ke\ e^2)$ proportional to $1/\rho_s$

As the Spaticle field density increases, m_e_vss increases and the equilibrium radius a_0 contracts proportionally. When ρ_s increases without bound:

$\rho_s \to$ infinity $\Rightarrow$ m_e_vss $\to$ infinity $\Rightarrow$ equilibrium radius $a_0 \to 0$, until atomic structure ceases to remain physically distinct from the nucleus $\Rightarrow$ electron-proton equilibrium destroyed. Conversely, as ρ_s decreases toward zero, m_e_vss decreases and a_0 grows without bound: atoms expand, not collapse, and the substrate condensation that constitutes the electron itself becomes vanishingly light

The collapse cascade, triggered by increasing ρ_s, proceeds in a specific order. Smaller-scale, weaker-energy structures fail first because they are more sensitive to fractional changes in the equilibrium radius. The complete sequence:

Spaticle field density rises; equilibrium radius a_0 contracts; van der Waals forces fail first; hydrogen bonds fail next; covalent bonds fail; electron-proton equilibrium is destroyed; hydrogen atom collapses toward nuclear scale; chemistry ceases; macroscopic matter loses structural integrity; stars, planets, and biological structures disappear.

The tolerance behaviour is strongly asymmetric. Downward variation in ρ_s permits substantial reduction before atomic collapse becomes a concern: a_0 grows instead of shrinking, and matter persists in an expanded but still organised form across many orders of magnitude of reduction. Upward variation is far more restrictive, because a_0 proportional to $1/\rho_s$ and bond energy proportional to $1/a_0^2$ together mean bond energies rise as ρ_s^2. Approximately 39% increase above the physical value begins disrupting van der Waals forces. Approximately 177% increase destroys hydrogen-bond structures. Approximately 11 to 13 times the physical value disrupts covalent bond structures. The physical value of ρ_s therefore occupies a tightly constrained chemistry-supporting region bounded from above: a relatively small fractional increase is sufficient to break the molecular and atomic structures that chemistry and biology require. It is not located at an arbitrary position within a wide allowed range. [P25 sensitivity table]

The decisive feature of this argument is that it does not depend on formation history. Grant the Big Bang or any existing matter distribution. The matter-stability condition still holds. Already-existing matter cannot survive a sufficiently large increase in substrate density. A substrate-density excursion of only a few hundred percent approaches a regime where stable chemistry and ordinary atomic structure can no longer be maintained.

---

8. The Persistent Deformation Mechanism

8.1 Physical Mechanism and Finite Deformation Domains

The finite deformation-domain structure is established in P18. It is separate from the observational DME law used for organised galactic rotation and KiDS-1000 weak lensing.

P18 defines the deformation-domain radius for a mass M as:

$Rd = (3M / (8\pi\rho_s))^{1/3}$.

This finite-domain relation fixes the characteristic domain scale once M and ρ_s are specified.

P18 also defines a rotationally enlarged domain radius:

$R\_eff = Rd\ (1 + vrot^2/c^2)^{1/3}$.

At galactic rotation speeds the correction is negligible, and P18 explicitly states that R_eff is not used in the DME equation.

The carrier field itself is governed by the covariant F1-cov equation in P18. Its static screening scale is determined by:

$m_{eff}^2 = 3G\rho_s/c^2 = 1/L_s^2$, with $L_s = c/(3G\rho_s)^{1/2}$.

The cosmological screening length Ls is distinct from the equilibrium carrier relaxation length $L_{rlx} \approx$ 45.17 AU and its corresponding τ_c.

P18 explicitly distinguishes the static F1-cov screening coefficient from the relaxation-diffusion coefficient. They are not interchangeable.

For the dark matter observations discussed here, the relevant organised-galaxy law is DME, not a Yukawa-domain fit to the SPARC or KiDS data.

The DME acceleration scale is fixed by the same substrate density:

$a_s = c\,(G\rho_s/3)^{1/2} = 1.20840317 \times 10^{-10}$ m s^{-2}.

The circular-speed form used for SPARC is:

$v^2(R) = v_b^2(R)\,[1 + a_s R / v_b^2(R)]^{1/2}$.

The corresponding extra-mass form is:

$M_{extra}(<R) = M_b(R)\,\{ [1 + a_s R^2/(G M_b(R))]^{1/2} - 1 \}$, with $M_b = v_b^2 R/G$.

No galaxy-specific gravity parameter is introduced. The same a_s is used for all SPARC galaxies.

For KiDS-1000, P18 uses the same DME equation and the same a_s, with $v_b^2(R) = G\,M_{gal}/R$ for the stack bins.

Thus the observational chain is: fixed ρ_s → fixed a_s → DME prediction. The DDR equation describes finite domain structure but is not the equation integrated to obtain the SPARC or KiDS DME results.

The finite-domain and carrier equations provide the underlying substrate framework, while DME is the standing regime law for the organised galactic and stack observations.

8.2 The DME Equation: Galactic Validation Across All Scales

The rotational deformation described in 8.1 is quantified for real galaxies by the DME equation of Paper 18. The acceleration is $a_s = c\,(G\rho_s/3)^{1/2} = 1.20840317 \times 10^{-10}$ m s^{-2}. The circular-speed form is $v^2(R) = v_b^2(R)\,[1 + a_s R/v_b^2(R)]^{1/2}$.

SPARC Validation: DME

Applied to all 175 galaxies in the SPARC database with Y = 0.5 at 3.6 μm and a_s from ρ_s: shape agreement 92.0%, flat classification 98.8%, non-flat classification 14.3%, median outer relative residual 0.100. Full per-galaxy results are Paper 18 Appendix A.

Extra Systems Under DME

Four independently sourced systems were tested using real, published measurements, not illustrative values.

FCC 224 (Buzzo et al.): ultra-diffuse galaxy, stellar mass $1.7 \cdot 10^8$ Msun, velocity dispersion 6 to 8 km/s. Organised rotation is negligible, so DME extra mass is negligible. The galaxy is independently reported as dark-matter-poor.

NGC 1277 (Comeron et al. 2023): compact relic galaxy, stellar mass $1.6 \cdot 10^{11}$ Msun, effective radius 1.2 kpc. Independently measured dark-matter fraction at 5 effective radii is below 5% at 2-sigma (Comeron et al. 2023). Under DME, extra mass tracks organised rotation and remains a partial check, as in Paper 18 Appendix D.

DLA0817g at z = 4.26 (Neeleman et al.): flat rotation curve at 272 km/s confirmed by ALMA, published dynamical mass log10(Mdyn) = 10.9. DME applies the same a_s as SPARC. Detail is Paper 18 Appendix D.

El Gordo (ACT-CL J0102-4915, Menanteau et al.), z = 0.87: member galaxies retain organised rotation through the collision and keep DME extra mass. The hot intracluster gas is stripped of organised motion. Lensing mass is observed to follow the galaxies, not the gas.

Two further systems, NGC 1052-DF2 and NGC 1052-DF4, were tested across the full range of disputed published velocity dispersion measurements for DF2 (3.2 to 9.5 km/s) and found to give consistently negligible extra mass (0.00 to 0.09%) across that entire range, not dependent on which disputed value is used.

9. The Identification

The same substrate density $\rho_s = 7.3 \times 10^{-27}$ kg/m³ runs through the ten cross-sectors, with results including the particle and electroweak sector, galaxy rotation curves, weak gravitational lensing, hydrogen atomic stability, the matter-stability condition, the vacuum-energy relation $u\_vac = \rho_s \cdot c^2$, and the H-class mass relation. Galaxy cluster dynamics and the Bullet Cluster provide additional observational consistency checks. The dark matter identification is presented as a consequence of a substrate density established independently of those astrophysical tests.

The Spaticle field satisfies every operational property historically attributed to dark matter:

Gravitationally active: The substrate deformation produced by rotating matter is gravitationally active through the DDR domain equation. It contributes to the total gravitational field.

Non-electromagnetic: The substrate does not emit, absorb, or scatter photons. It is invisible to all electromagnetic observatories. This is not a property introduced to explain observations. It follows from P14.

Non-baryonic: The substrate is not composed of baryons. It is the medium in which baryons are themselves organised condensations.

Spatially extended: The substrate deformation extends to Rd, which for galactic masses is of order 1 Mpc. This produces the extended gravitational influence attributed to dark matter halos.

Clustered with matter: The substrate deformation is sourced by matter distributions. It clusters where matter clusters.

Passes through collisions: Non-electromagnetic substrate is not decelerated by ram pressure in cluster collisions, consistent with the Bullet Cluster observation.

Beyond these operational equivalences, the Spaticle field does what no dark matter candidate has ever done: it explains particle masses, coupling relations, atomic structure, and cosmic gravitational dynamics from one substrate density with no free parameters. A WIMP was introduced as a dark matter candidate for gravitational anomalies alone, whereas the Spaticle field connects particle and gravitational sectors simultaneously. The Spaticle field was derived from particle physics and reproduces astrophysical observations as a consequence.

---

10. Falsifiable Predictions

> Prediction 1: Domain-boundary transitions in galaxy rotation curves at large radii where the galactic domain terminates and the cluster background takes over. Observable as a steeper-than-Keplerian decline followed by a floor set by the cluster potential.
>
> Prediction 2: Weak lensing signal consistent with DDR domain structure, not NFW profiles, across all future lensing surveys.
>
> Prediction 3: The four-unit condensation has two higher configuration resonances. The 2+2 excitation gives the Shankar resonance, $m_{Shankar} c^2 = 2.60 E_{unit} = 776.5$ MeV. The 4+0 excitation gives the BFUT resonance, $m_{BFUT} c^2 = 4.70 E_{unit} = 1403.7$ MeV. P16A gives the full derivation and resonance correspondence.
>
> Prediction 4: Progressive discovery of larger nested rotational hierarchies predicted by DDR hierarchical domain structure, beyond currently confirmed scales, as improved peculiar-velocity surveys extend the basin-of-attraction mapping.
>
> Prediction 5: Continued null results in direct detection experiments for particulate dark matter candidates are expected if the observed gravitational effects arise from substrate deformation, not particulate dark matter. The substrate is not particulate and is not expected to produce particulate direct-detection signatures in WIMP, axion, or sterile neutrino search experiments.

10.1 Foundational Principles and Derived Consequences

Every major physical theory begins from foundational principles that are postulated and subsequently tested through derived consequences.

Newton postulated gravitational attraction before deriving planetary motion: $F = G\, m1\, m2 / r^2$. General relativity introduced spacetime curvature as a foundational principle before deriving relativistic effects. Quantum mechanics introduced the wavefunction before deriving atomic structure. Quantum field theory assumes universal fields before deriving interactions among excitations.

Within the present framework the Spaticle substrate and its organisational principles occupy the foundational role. The relevant test is whether the distinct derivational chains survive comparison with observation.

---

11. Conclusion

Dark matter is identified with the Spaticle field through convergence across the ten cross-sectors on a single substrate density $\rho_s = 7.3 \times 10^{-27}$ kg/m³, with results including particle and electroweak structure, galaxy rotation curves across 175 SPARC galaxies, KiDS-1000 weak gravitational lensing, hydrogen atomic stability derived from first principles, the matter-stability condition, the vacuum-energy relation $u_{vac} = \rho_s \cdot c^2$, and the H-class mass relation. Galaxy cluster dynamics and the Bullet Cluster provide additional observational consistency checks.

ρ_s is the common substrate parameter that propagates through the independently established BFUT derivation chain, together with the explicitly identified measured anchors (including mp and rp) that each sector's SI calibration requires.
The dark matter programme correctly identified real gravitational anomalies across decades of careful observation. Its error was not observational. Its error was ontological: it assumed the gravitational excess must consist of undiscovered particles. The same substrate density ρ_s that governs these sectors is

additionally consistent with every other dark matter evidence class: galaxy cluster velocity dispersions (Zwicky evidence), CMB temperature and acoustic peak structure (P7, P7A), Big Bang Nucleosynthesis constraints which dissolve in the steady-state nucleosynthesis framework (P3), and the Sunyaev-Zeldovich effect, ISW effect, Lyman-alpha forest, and weak lensing S8 tension (P10-P13). The Spaticle field is not a particle. It is the physical medium of space itself. The gravitational anomalies the dark matter programme detected are the persistent rotational deformation of this medium by rotating baryonic matter.

The same substrate density participates across electroweak structure, particle hierarchy, domain formation, galaxy dynamics, weak lensing, gravitational-wave persistence, hydrogen structure, and chemistry. A successful application in one isolated sector would be insufficient. What is present here is the same fixed quantity participating simultaneously across independent sectors spanning approximately forty orders of magnitude in physical scale. Explaining away the dark matter identification requires an alternative account of why one number simultaneously reproduces all of these. [P16, P17, P18, P19, Paper 19, P25]

The Standard Model requires 19 independent measured parameters, none derived from any other. The BFUT framework reproduces coupling constants through substrate organisation and fixes the physical scale through one substrate density constrained independently across ten sectors. Pull back from the hydrogen atom to the galaxy cluster to the cosmic web: at every level of this fractal zoom, the same $\rho_s = 7.3 \times 10^{-27}$ kg/m³ holds. Dark matter is not a twentieth mystery. It is a consequence of the same substrate from which the first nineteen are derived.

The standing DME galaxy-rotation and KiDS-1000 results use the same parameter-free acceleration scale a_s derived from ρ_s. The finite-domain DDR relation remains a separate structural relation and is not the equation used to generate the SPARC or KiDS DME results.

Appendix: Simulation Code

A3. Galaxy Rotation, Lensing, and GW Simulations

Full simulation code, data, figures, and README files for galaxy rotation curve fitting (175 SPARC galaxies), KiDS-1000 weak lensing validation, domain boundary profiling, and peculiar velocity consistency are deposited at:

Zenodo DOI: 10.5281/zenodo.20517866 (full five-term functional, 3+1 robustness scans, partition energy analysis, parameter space coverage)

Full DME validation details are given in Paper 18 Appendix A and Paper 33. The separate DDR simulation material is not used for the DME results reported here.

Appendix A. SPARC validation under DME

This appendix reports DME on all 175 galaxies in the SPARC database (Lelli, McGaugh and Schombert 2016). Υ = 0.5 at 3.6 μm. a_s is computed from ρ_s.

A1. Formula (DME)

$a_s = c\,(G\,\rho_s / 3)^{1/2} = 1.20840317 \times 10^{-10}$ m s^{-2}, with $\rho_s = 7.3 \times 10^{-27}$ kg m^{-3}.

Baryonic input: $v_b^2(R) = v_{gas}|v_{gas}| + \Upsilon\, v_{disk}^2 + \Upsilon\, v_{bulge}^2$.

DME: $v^2(R) = v_b^2(R)\,[1 + a_s R / v_b^2(R)]^{1/2}$.
Equivalent extra mass: $M_{extra}(<R) = M_b(R)\,\{\,[1 + a_s R^2/(G\,M_b(R))]^{1/2} - 1\,\}$, with $M_b = v_b^2 R/G$.

Flat classification: outer-half scatter (std/mean) < 0.12.

A2. Summary results

N = 175 galaxies.

- Shape agreement (flat versus non-flat): 92.0% (161/175)
- Flat correct: 98.8% (159/161)
- Non-flat correct: 14.3% (2/14)
- Median outer relative residual: 0.096
- Fraction with outer relative residual < 0.20: 76.0%
- Fraction with outer relative residual < 0.25: 84.6%

A3. Second-level note on non-flat failures

Of galaxies observed non-flat but predicted flat, the large majority have a baryonic curve Vbar that is already flat under the same outer-scatter rule. The non-flat recovery ceiling is therefore largely structural: non-negative extra mass cannot force a declining shape when Vbar itself is flat.

A4. Full galaxy table

Columns: Galaxy; N points; Mbar; Vchar; observed flat; predicted flat; shape correct; median outer relative residual.

Galaxy	N	Mb / M_{sun}	V_{char}	ObsF	PredF	Shape	Med|rel|
CamB	9	6.613e+07	14.7	N	Y	N	1.039
D512-2	4	2.378e+08	35.9	Y	Y	Y	0.088
D564-8	6	5.626e+07	24.0	Y	Y	Y	0.214
D631-7	16	5.597e+08	57.0	Y	Y	Y	0.070
DDO064	14	4.432e+08	46.3	Y	Y	Y	0.043
DDO154	12	3.637e+08	46.3	Y	Y	Y	0.009
DDO1	31	2.926e	65.6	Y	Y	Y	0.218

61		+09					
DDO168	10	6.237e+08	52.5	Y	Y	Y	0.045
DDO170	8	2.129e+09	59.0	Y	Y	Y	0.201
ESO079-G014	15	3.626e+10	172.5	Y	Y	Y	0.125
ESO116-G012	15	5.208e+09	109.0	Y	Y	Y	0.173
ESO444-G084	7	2.775e+08	62.7	Y	Y	Y	0.286
ESO563-G021	30	2.148e+11	315.0	Y	Y	Y	0.199
F561-1	6	4.668e+09	49.8	Y	N	N	0.615
F563-1	17	6.975e+09	111.0	Y	Y	Y	0.181
F563-V1	6	1.242e+09	28.6	Y	Y	Y	1.140
F563-V2	10	5.549e+09	117.5	Y	Y	Y	0.198
F565-V2	7	1.861e+09	76.0	Y	Y	Y	0.146
F567-2	5	2.526e+09	48.1	Y	N	N	0.432
F568-1	12	1.075e+10	130.0	Y	Y	Y	0.263
F568-3	18	1.137e+10	104.0	Y	Y	Y	0.036
F568-V1	15	7.570e+09	112.0	Y	Y	Y	0.188
F571-8	13	6.014e+09	140.0	Y	Y	Y	0.311
F571-V1	7	3.737e+09	83.2	Y	Y	Y	0.022
F574-1	14	6.330e+09	97.8	Y	Y	Y	0.100
F574-2	5	3.659e+09	36.0	Y	Y	Y	1.152
F579-V1	14	1.097e+10	114.0	Y	Y	Y	0.055
F583-1	25	6.466e+09	85.8	Y	Y	Y	0.125
F583-4	12	1.556e+09	62.1	Y	Y	Y	0.036
IC2574	34	2.439e+09	55.9	N	Y	N	0.198

IC4202	32	1.246e+11	244.5			Y	Y	Y	0.106
KK98-251	15	2.770e+08	32.6			Y	Y	Y	0.296
NGC0024	29	3.408e+09	107.5			Y	Y	Y	0.214
NGC0055	21	7.162e+09	85.4			Y	Y	Y	0.133
NGC0100	21	2.847e+09	85.3			Y	Y	Y	0.092
NGC0247	26	8.105e+09	103.5			Y	Y	Y	0.015
NGC0289	28	9.043e+10	173.5			Y	Y	Y	0.103
NGC0300	25	3.249e+09	91.1			Y	Y	Y	0.111
NGC0801	13	2.363e+11	216.0			Y	Y	Y	0.130
NGC0891	18	8.514e+10	219.0			Y	Y	Y	0.040
NGC1003	36	1.331e+10	109.0			Y	Y	Y	0.039
NGC1090	24	5.868e+10	165.0			Y	Y	Y	0.039
NGC1705	14	5.493e+08	71.5			Y	Y	Y	0.285
NGC2366	26	1.092e+09	50.7			Y	Y	Y	0.158
NGC2403	73	1.284e+10	134.0			Y	Y	Y	0.120
NGC2683	11	5.021e+10	157.5			Y	Y	Y	0.044
NGC2841	50	1.651e+11	283.0			Y	Y	Y	0.232
NGC2903	34	4.814e+10	185.5			Y	Y	Y	0.092
NGC2915	30	1.250e+09	81.8			Y	Y	Y	0.252
NGC2955	24	2.138e+11	255.5			Y	Y	Y	0.035
NGC2976	27	1.902e+09	75.4			N	Y	N	0.042
NGC2998	13	1.240e+11	213.0			Y	Y	Y	0.035
NGC3109	25	6.844e+08	61.2			Y	Y	Y	0.154
NGC3198	43	4.299e+10	149.0			Y	Y	Y	0.037
NGC3521	41	5.312e+10	206.0			Y	Y	Y	0.136
NGC3	12	5.203e	167.5			Y	Y	Y	0.014

726		+10					
NGC3741	21	3.036e+08	49.2	Y	Y	Y	0.103
NGC3769	12	1.805e+10	118.0	Y	Y	Y	0.081
NGC3877	13	4.993e+10	169.0	Y	Y	Y	0.053
NGC3893	10	4.030e+10	179.0	Y	Y	Y	0.097
NGC3917	17	1.740e+10	137.0	Y	Y	Y	0.064
NGC3949	7	2.337e+10	163.0	Y	Y	Y	0.046
NGC3953	8	9.252e+10	223.0	Y	Y	Y	0.039
NGC3972	10	1.049e+10	126.5	Y	Y	Y	0.123
NGC3992	9	1.548e+11	242.0	Y	Y	Y	0.090
NGC4010	12	1.268e+10	124.0	Y	Y	Y	0.048
NGC4013	36	5.361e+10	172.0	Y	Y	Y	0.050
NGC4051	7	4.482e+10	157.0	Y	Y	Y	0.115
NGC4068	6	3.522e+08	36.0	N	Y	N	0.248
NGC4085	7	1.486e+10	131.5	Y	Y	Y	0.023
NGC4088	12	7.618e+10	171.0	Y	Y	Y	0.162
NGC4100	24	3.940e+10	176.0	Y	Y	Y	0.086
NGC4138	7	2.534e+10	148.5	Y	Y	Y	0.048
NGC4157	17	7.076e+10	184.0	Y	Y	Y	0.016
NGC4183	23	1.218e+10	110.0	Y	Y	Y	0.047
NGC4214	14	8.518e+08	80.4	Y	Y	Y	0.266
NGC4217	19	4.807e+10	184.5	Y	Y	Y	0.042
NGC4389	6	1.276e+10	89.7	N	Y	N	0.442
NGC4559	32	2.340e+10	122.0	Y	Y	Y	0.064
NGC5005	18	1.043e+11	264.0	Y	Y	Y	0.076
NGC5033	22	8.040e+10	197.5	Y	Y	Y	0.058

NGC5055	28	9.897e+10	179.5	Y	Y	Y	0.089
NGC5371	19	2.361e+11	213.0	Y	Y	Y	0.161
NGC5585	24	4.239e+09	89.9	Y	Y	Y	0.058
NGC5907	19	1.391e+11	215.5	Y	Y	Y	0.010
NGC5985	33	1.546e+11	290.5	Y	Y	Y	0.244
NGC6015	44	2.984e+10	158.5	Y	Y	Y	0.092
NGC6195	23	2.351e+11	254.5	Y	Y	Y	0.032
NGC6503	31	1.005e+10	115.0	Y	Y	Y	0.046
NGC6674	15	1.502e+11	242.0	Y	Y	Y	0.100
NGC6789	4	6.095e+07	53.5	N	Y	N	0.430
NGC6946	58	4.524e+10	163.0	Y	Y	Y	0.023
NGC7331	36	1.602e+11	238.0	Y	Y	Y	0.029
NGC7793	46	5.935e+09	108.0	Y	Y	Y	0.085
NGC7814	18	4.121e+10	214.0	Y	Y	Y	0.234
PGC51017	6	2.589e+08	18.3	Y	Y	Y	1.317
UGC00128	22	2.343e+10	131.0	Y	Y	Y	0.028
UGC00191	9	3.822e+09	82.4	Y	Y	Y	0.033
UGC00634	4	7.183e+09	107.5	Y	Y	Y	0.075
UGC00731	12	3.451e+09	73.6	Y	Y	Y	0.090
UGC00891	5	9.939e+08	60.1	Y	Y	Y	0.029
UGC01230	11	1.846e+10	103.0	Y	Y	Y	0.228
UGC01281	25	6.785e+08	54.1	Y	Y	Y	0.066
UGC02023	5	9.206e+08	47.9	N	Y	N	0.172
UGC02259	8	2.316e+09	86.0	Y	Y	Y	0.148
UGC02455	8	2.825e+09	48.5	N	Y	N	0.709
UGC0	17	2.957e	332.0	Y	Y	Y	0.219

2487		+11							
UGC02885	19	3.540e+11	298.0			Y	Y	Y	0.095
UGC02916	43	1.120e+11	196.0			Y	Y	Y	0.076
UGC02953	115	1.556e+11	264.0			Y	Y	Y	0.167
UGC03205	48	8.093e+10	215.0			Y	Y	Y	0.108
UGC03546	30	6.270e+10	193.5			Y	Y	Y	0.068
UGC03580	47	1.469e+10	124.5			Y	Y	Y	0.031
UGC04278	25	3.223e+09	80.0			N	N	Y	0.173
UGC04305	22	1.417e+09	33.1			Y	Y	Y	0.895
UGC04325	8	2.456e+09	91.5			Y	Y	Y	0.177
UGC04483	8	5.031e+07	23.5			Y	Y	Y	0.191
UGC04499	9	3.024e+09	72.8			Y	Y	Y	0.033
UGC05005	11	1.235e+10	99.2			Y	Y	Y	0.084
UGC05253	73	1.186e+11	218.0			Y	Y	Y	0.055
UGC05414	6	1.084e+09	56.8			Y	Y	Y	0.060
UGC05716	12	2.534e+09	73.0			Y	Y	Y	0.057
UGC05721	23	1.217e+09	78.4			Y	Y	Y	0.211
UGC05750	11	9.132e+09	78.2			Y	Y	Y	0.230
UGC05764	10	3.768e+08	52.3			Y	Y	Y	0.160
UGC05829	11	2.251e+09	59.2			N	N	Y	0.109
UGC05918	8	4.031e+08	41.2			Y	Y	Y	0.037
UGC05986	15	4.268e+09	114.5			Y	Y	Y	0.224
UGC05999	5	1.043e+10	97.7			Y	Y	Y	0.016
UGC06399	9	2.726e+09	84.1			Y	Y	Y	0.100
UGC06446	17	3.156e+09	82.1			Y	Y	Y	0.054
UGC06614	13	1.198e+11	203.0			Y	Y	Y	0.058

UGC06628	7	3.715e+09	42.3	Y	Y	Y	0.826
UGC06667	9	1.618e+09	84.0	Y	Y	Y	0.240
UGC06786	45	4.653e+10	224.0	Y	Y	Y	0.261
UGC06787	71	6.218e+10	248.0	Y	Y	Y	0.287
UGC06818	8	1.689e+09	68.1	N	Y	N	0.045
UGC06917	11	7.717e+09	103.0	Y	Y	Y	0.086
UGC06923	6	2.754e+09	78.8	Y	Y	Y	0.025
UGC06930	10	1.165e+10	108.0	Y	Y	Y	0.049
UGC06973	9	3.062e+10	175.5	Y	Y	Y	0.059
UGC06983	17	8.775e+09	108.5	Y	Y	Y	0.053
UGC07089	12	3.689e+09	72.8	Y	Y	Y	0.139
UGC07125	13	7.625e+09	65.1	Y	Y	Y	0.529
UGC07151	11	2.488e+09	71.9	Y	Y	Y	0.031
UGC07232	4	8.738e+07	35.2	N	Y	N	0.082
UGC07261	7	2.319e+09	74.1	Y	Y	Y	0.039
UGC07323	10	3.623e+09	77.5	N	Y	N	0.031
UGC07399	10	1.618e+09	98.5	Y	Y	Y	0.345
UGC07524	31	4.794e+09	77.0	Y	Y	Y	0.058
UGC07559	7	2.296e+08	30.4	Y	Y	Y	0.277
UGC07577	9	6.037e+07	14.1	N	Y	N	1.038
UGC07603	12	4.906e+08	61.5	Y	Y	Y	0.183
UGC07608	8	7.935e+08	63.7	Y	Y	Y	0.191
UGC07690	7	9.476e+08	57.4	Y	Y	Y	0.055
UGC07866	7	1.830e+08	29.4	Y	Y	Y	0.250
UGC08286	17	1.997e+09	82.9	Y	Y	Y	0.164
UGC0	30	1.715e	79.2	Y	Y	Y	0.134

8490		+09							
UGC08550	11	7.564e+08	56.2			Y	Y	Y	0.112
UGC08699	41	3.422e+10	180.0			Y	Y	Y	0.152
UGC08837	8	8.396e+08	44.8			Y	Y	Y	0.235
UGC09037	22	6.316e+10	154.5			Y	Y	Y	0.119
UGC09133	68	2.097e+11	228.0			Y	Y	Y	0.039
UGC09992	5	4.985e+08	33.4			Y	Y	Y	0.493
UGC10310	7	2.849e+09	71.7			Y	Y	Y	0.081
UGC11455	36	2.539e+11	272.0			Y	Y	Y	0.048
UGC11557	12	1.041e+10	81.6			Y	Y	Y	0.347
UGC11820	10	5.135e+09	79.1			Y	Y	Y	0.106
UGC11914	65	7.692e+10	284.0			Y	Y	Y	0.181
UGC12506	31	1.581e+11	238.5			Y	Y	Y	0.139
UGC12632	15	3.331e+09	70.8			Y	Y	Y	0.077
UGC12732	16	7.673e+09	86.8			Y	Y	Y	0.049
UGCA 281	7	6.001e+07	28.1			Y	Y	Y	0.035
UGCA 442	8	5.759e+08	56.5			Y	Y	Y	0.061
UGCA 444	36	1.404e+08	33.0			Y	Y	Y	0.105

End of Appendix A. Data source: SPARC (Lelli et al. 2016). Computations: DME with a_s from ρ_s. Per-galaxy DME residuals are tabulated in Paper 18 Appendix A and Paper 33.

Appendix B. KiDS-1000 weak lensing under DME

This appendix reports DME on the KiDS-1000 stacked weak-lensing products from Brouwer et al. (2021), four stellar-mass bins.

B1. Formula (DME)

The same equation and the same a_s as Appendix A.

$$a_s = 1.20840317 \times 10^{-10}\ \mathrm{m\ s^{-2}}$$

$$v_b^2(R) = G\,M_{gal} / R$$

$$v^2(R) = v_b^2(R)\,[1 + a_s\,R / v_b^2(R)]^{1/2}$$

$\rho_s = 7.3 \times 10^{-27}$ kg m^{-3}

No disk core term. Difference from SPARC is only the baryonic input.

Deep-regime floor:

$$v^4 = G\, M_{gal}\, a_s$$

Equivalent circular speed from ESD: $v^2 = 2 \pi G \Delta\Sigma R$ when that conversion is used.

Mgal is the Brouwer et al. (2021) bin mean for stars plus cold gas.

ESD profiles are the observational input. Radii beyond Rd require nested-domain organisation $N(\Sigma_i)$.

B2. Data

Source: KiDS-1000 / Brouwer et al. (2021) public products. a_s is not fitted per bin.

B3. Results

- Same a_s in every bin. Flat equivalent-speed ranking and M^{1/4} mass scaling inside one domain.
- No per-bin retuning.

Amplitude outside Rd is assigned to nested-domain organisation.

These results are the standing KiDS test under DME.

B4. Relation to SPARC

SPARC and KiDS use the same DME equation and the same a_s. The difference is only the baryonic input: resolved vb(R) versus G Mgal / R.

Appendix C. Standard QFT vacuum energy, the two ontological corrections, and the substrate-density account of the cosmological constant problem

Vijay Shankar Sharma | ORCID: 0009-0001-9622-6121 |

D.1 Purpose

This appendix provides a technical account of the standard quantum field theory (QFT) calculation of vacuum energy density, the two specific ontological corrections introduced in the BFUT framework, and the resolution of the cosmological constant problem that follows. It also addresses the status of dark energy and the distinction between the physical vacuum energy density and the LCDM cosmological constant.

D.2 The Standard QFT Vacuum Energy Calculation

In standard QFT the vacuum energy density is obtained by summing the zero-point energy of all modes of all quantum fields up to a high-energy cutoff, conventionally the Planck scale:

$$\rho\_QFT \approx \Sigma\_fields \int d^3k/(2\pi)^3 \times (½\, \hbar\, \omega\_k)$$

The sum runs over all particle species - approximately 17 independent fields in the Standard Model counting degrees of freedom. Each mode contributes zero-point energy $\frac{1}{2}\hbar\omega_k$. The integral yields:

Cosmological observations infer an effective energy density of order 10^{-10} J/m³. The standard cutoff estimate therefore differs by roughly 120 to 122 orders of magnitude. This is the conventional cosmological constant problem.

D.3 The Two Ontological Corrections to the Standard QFT Treatment

Correction 1 - Multiplicity of independent quantum fields.

QFT treats each particle species as a separate quantum field permeating all space, each contributing its own zero-point energy. This results in a sum over approximately 17 distinct fields. In the BFUT framework there is one underlying physical medium, the Spaticle substrate, of which every particle and every force carrier is an organised excitation. There are not 17 independent vacuum energies. There is one substrate.

Correction 2 - Zero-point energy assigned to empty modes.

QFT assigns $\frac{1}{2}\hbar\omega$ to every mode of every field regardless of whether that mode contains any physical excitation. In the BFUT ontology, $\frac{1}{2}\hbar_{vss}\omega$ is the minimum internal circulation energy of an organised condensation. It is a property of matter, not of empty space. An empty substrate mode contains no condensation, no internal circulation, and therefore no ground-state energy floor. Empty modes contribute zero.

D.4 Application of the BFUT Corrections

With one underlying physical medium and zero-point energy assigned only to actual organised condensations, every unoccupied mode contributes zero. For the pure vacuum state, containing no organised condensations, the corrected QFT mode sum therefore vanishes:

$$\rho_{QFT,corrected} = 0$$

This removes the contribution that produced the conventional discrepancy exceeding 120 orders of magnitude. It does not calculate the rest energy of the physical substrate. That is a separate particle-sector result: $u_s = \rho_s c^2 = 6.56 \times 10^{-10}$ J/m³.

D.5 Separate Physical Result: Equilibrium Substrate Rest Energy

The substrate rest-energy density follows directly from the particle-derived equilibrium mass density by mass-energy equivalence:

$$u_s = \rho_s c^2 = 6.56 \times 10^{-10} \text{ J/m}^3$$

The two statements have different meanings. The corrected QFT empty-mode sum is zero, while the one real substrate has a finite equilibrium rest-energy density. They must not be presented as two derivations of the same number.

D.6 Particle-Sector Origin and Downstream Applications of ρs

The equilibrium density used here is derived once in the particle sector. With m*_vss = m_e_vss/α_vss and r_e_vss = α_vss·ħ_vss/(m_e_vss·c), the Einstein-normalised gravitational self-energy density gives:

$$\rho s = [Gc^2/(8\pi\hbar\_vss^4)](m\_e\_vss/\alpha\_vss)^6 = 7.30 \times 10^{-27}\ \text{kg/m}^3$$

Galaxy dynamics, lensing, gravity, time, atomic structure, and other sectors are downstream applications or tests. They do not independently determine ρs in this revision. A result changes numerically only if ρs survives in its final equation.

D.7 Dark Energy, the Cosmological Constant, and the Λ Tension

The cosmological expression $\rho\_\Lambda = 3\Omega\_\Lambda H_0^2/(8\pi G)$ depends on the adopted value of H_0. Its representative value is stated once in Section 2 and is retained only as an independent comparison.
The particle-sector result is 7.30×10^{-27} kg/m³, corresponding to 6.56×10^{-10} J/m³. It is 23.7% higher, a separation of 0.092 orders of magnitude. This is an order-of-magnitude proximity, not exact equality. The comparison is also qualitatively different from the conventional QFT estimate because the corrected pure-vacuum mode sum has already collapsed to zero under the one-field, no-empty-zero-mode ontology.
BFUT may continue to interpret apparent cosmic acceleration through large-scale kinematics rather than a separate dark-energy substance. That interpretation is independent of the particle-sector derivation of ρs.

D.8 Summary

The standard QFT vacuum estimate is removed by two ontological corrections: one physical field rather than many independent physical vacuum fields, and zero-point energy only for organised condensations rather than empty modes. The corrected pure-vacuum mode sum is therefore zero. Separately, the particle sector derives ρs = 7.30×10^{-27} kg/m³ and u_s = 6.56×10^{-10} J/m³. The H_0-dependent cosmological comparison stated in Section 2 is 23.7% lower. All other sectors are applications or tests, not independent derivations of the substrate density.

Appendix D

1. The Full Five-Term Functional

The BFUT condensation energy functional has five terms. Each term encodes a distinct physical mechanism. Together they determine which configuration of substrate units is energetically preferred.

The full functional evaluated for a configuration of n units with k co-rotating:

E = coop + imb + geom + c3ph

1.1 Term by Term

Term 1 - Cooperation (coop)

coop = -J x pairs_sum(s)

pairs_sum(s) = sum of s_i x s_j over all distinct pairs i < j

Physical meaning: Co-rotating units attract each other by the Bernoulli mechanism. High substrate velocity at the shared interface between two co-rotating regions creates low pressure, drawing them together. The cooperation energy grows with the number of co-rotating pairs.

k co-rotating	Pairs	Binding energy

1	0	0 (no pairs, unstable)
2	1	-J = -1.0 (marginal)
3	**3**	**-3J = -3.0 (qualitative jump - first stable nucleus)**
4	6	-6J = -6.0

The jump from k=2 (one pair, -J) to k=3 (three pairs, -3J) is qualitative not gradual. This is why the 3-core is the first stable nucleus. Below k=3 the core cannot survive substrate fluctuations.

Term 2 - Imbalance Penalty (imb)

imb = λ x $(\text{sum}(s))^2$

Physical meaning: A net circulation asymmetry costs energy. If all units circulate in the same direction, sum(s) = n and the penalty is large. The balanced 2+2 configuration has sum(s) = 0 and zero penalty. The 3+1 configuration has sum(s) = 3-1 = 2, giving a moderate penalty λ x 4 = 2.4.

Term 3 - Geometric Cost (geom)

geom = $(k-3)^2 + \alpha$ x (n-k)

Physical meaning: Two independent geometric costs. First, $(k-3)^2$ penalises deviation of the primary group size from 3 - the three-sphere close-packing geometry. Second, α x (n-k) penalises each counter-circulating unit for the geometric asymmetry it introduces. When the expelled unit has mass fraction μ, this term scales as α x μ.

Term 4 - Circulation Phase Reward (c3ph)

c3ph = D_s x cos(3 x φ)

Physical meaning: The fifth term explicitly encodes the topology of the three-sphere packing into the energy functional. The phase φ measures the circulation configuration:

Config	φ	cos(3φ)	c3ph = D_s x cos(3φ)	Effect
3+1	**π/3**	**-1**	**-D_s = -1.5**	**Rewarded**
2+2	π/2	0	0	Neutral
4+0	**0**	**+1**	**+D_s = +1.5**	**Penalised**

D_s must be positive. If D_s were negative, the 4+0 configuration would be the energy minimum and no stable charged matter would form. The fifth term raises E(4+0) from 4.60 to 6.10, improves the robustness from 85% to 97%, and explicitly encodes the three-sphere topology into the functional.

1.2 Parameters

Symbol	Value	Name	Physical role
J	1.0	Cooperation strength	Bernoulli binding per co-rotating pair
λ	0.6	Imbalance penalty	Cost of net circulation asymmetry
α	0.5	Geometric asymmetry	Cost per counter-circulating unit (scales with μ for expelled unit)
D_s	1.5	Phase reward	cos(3φ) circulation topology reward. Must be positive.

2. The Per-Unit Energy Scan (Code 1)

Code 1 answers: for n co-rotating substrate units, which n minimises energy per unit E(n)/n? All units are at the primary phase φ = π/3, so cos(3φ) = -1 and c3ph = -D_s for all n.

n	E(n)	E(n)/n	Note
1	3.1000	3.1000	No pairs. Unstable.
2	0.9000	0.4500	One pair. Marginal.
3	**0.9000**	**0.3000**	**MINIMUM E/unit. The 3-core attractor.**
4	3.1000	0.7750	
5	7.5000	1.5000	Rising steeply
6-12	...	...	Continues to rise

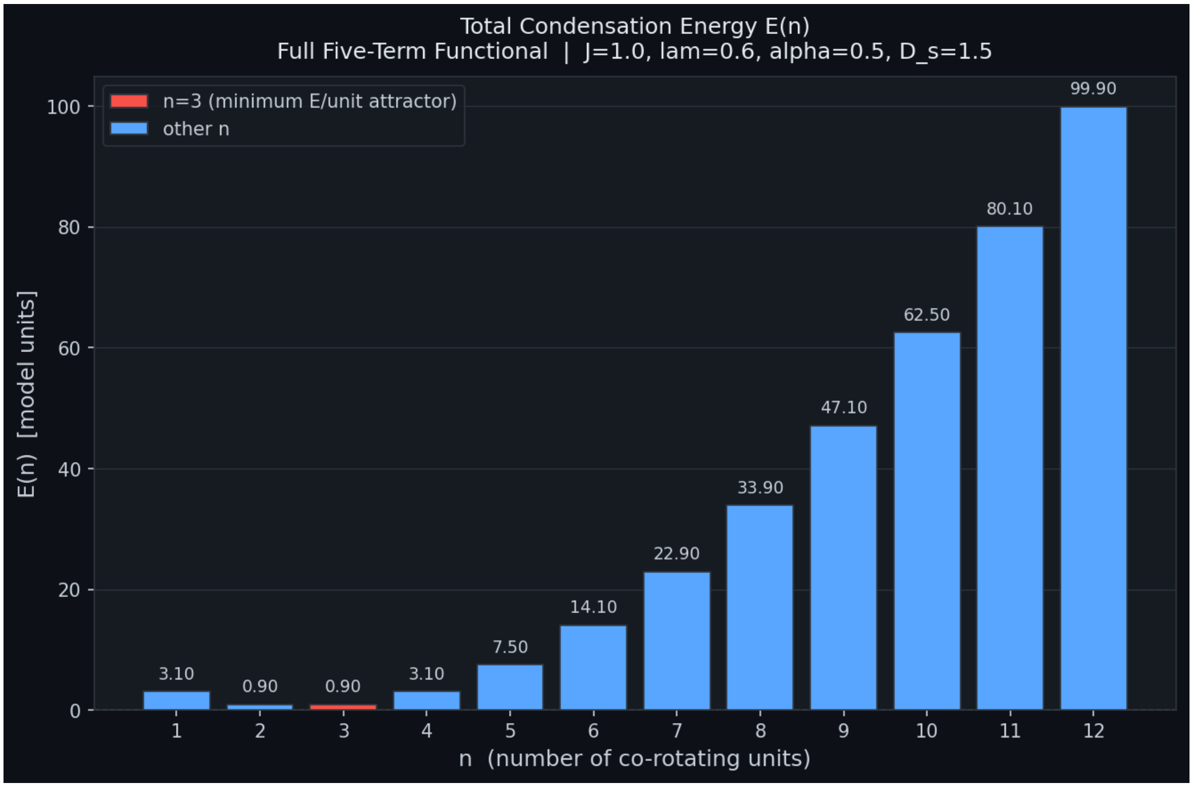

Figure A. Total condensation energy E(n) for n=1 to 12. n=3 highlighted.

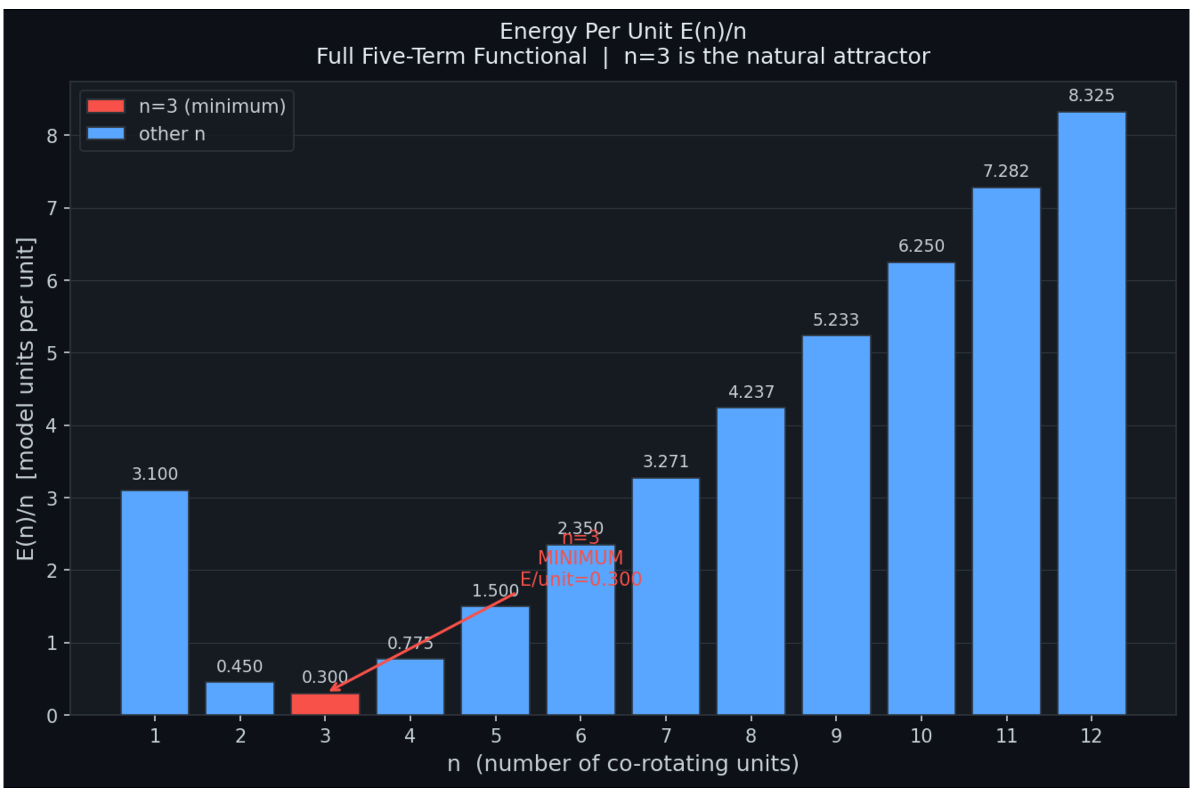

Figure B. Energy per unit E(n)/n for n=1 to 12. n=3 is the unambiguous minimum.

3. The Four-Unit Partition (Post 3-Core Formation)

The moment n=3 forms, the three-sphere packing geometry simultaneously creates the interstitial region. The four-unit bound system forms at E=1.400 model units. The three configurations and their full-functional energies:

Config	E (model units)	cos(3φ)	Status
3+1	**1.4000**	**-1 (rewarded)**	**MINIMUM. SELECTED.**
2+2	4.0000	0 (neutral)	Symmetric. No net charge.
4+0	**6.1000**	**+1 (penalised)**	**All co-rotating. Penalised by D_s.**

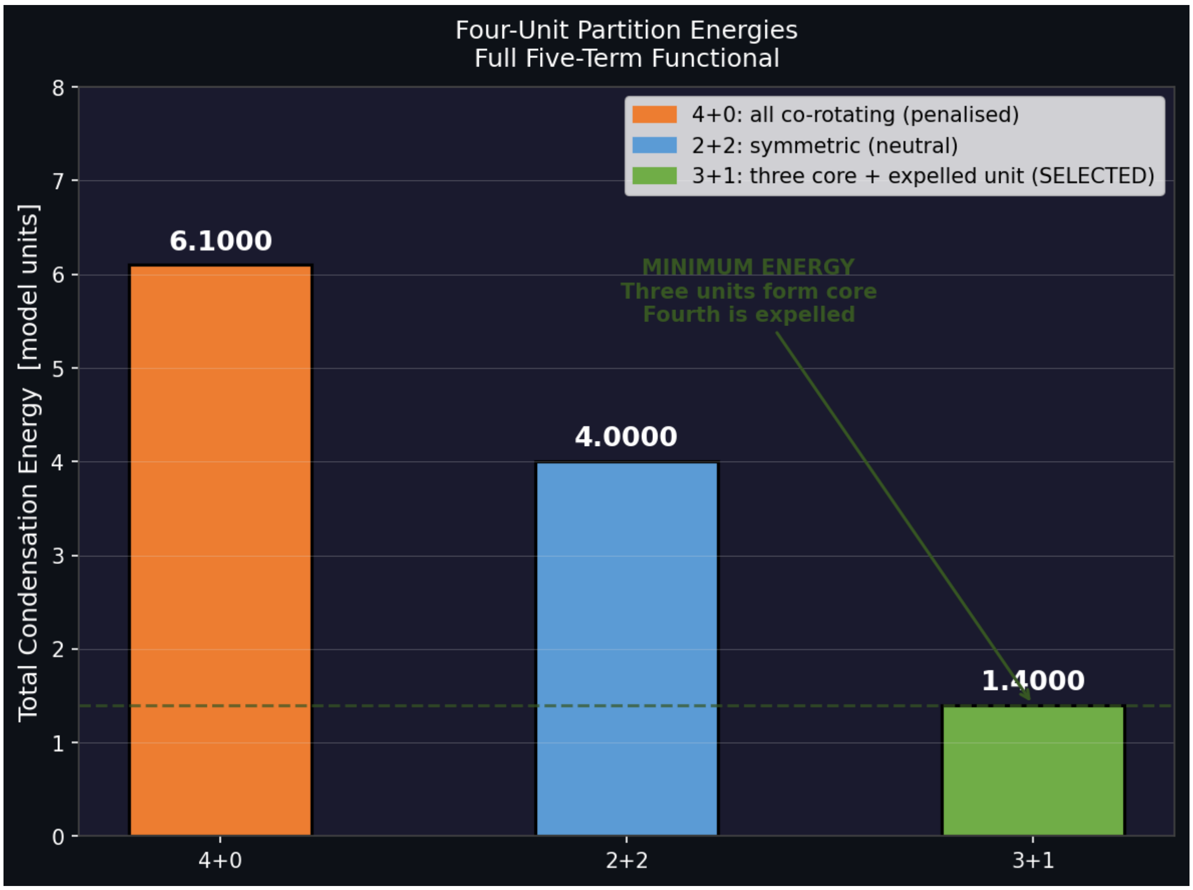

Figure C. Four-unit partition energies. 3+1 is the clear minimum.

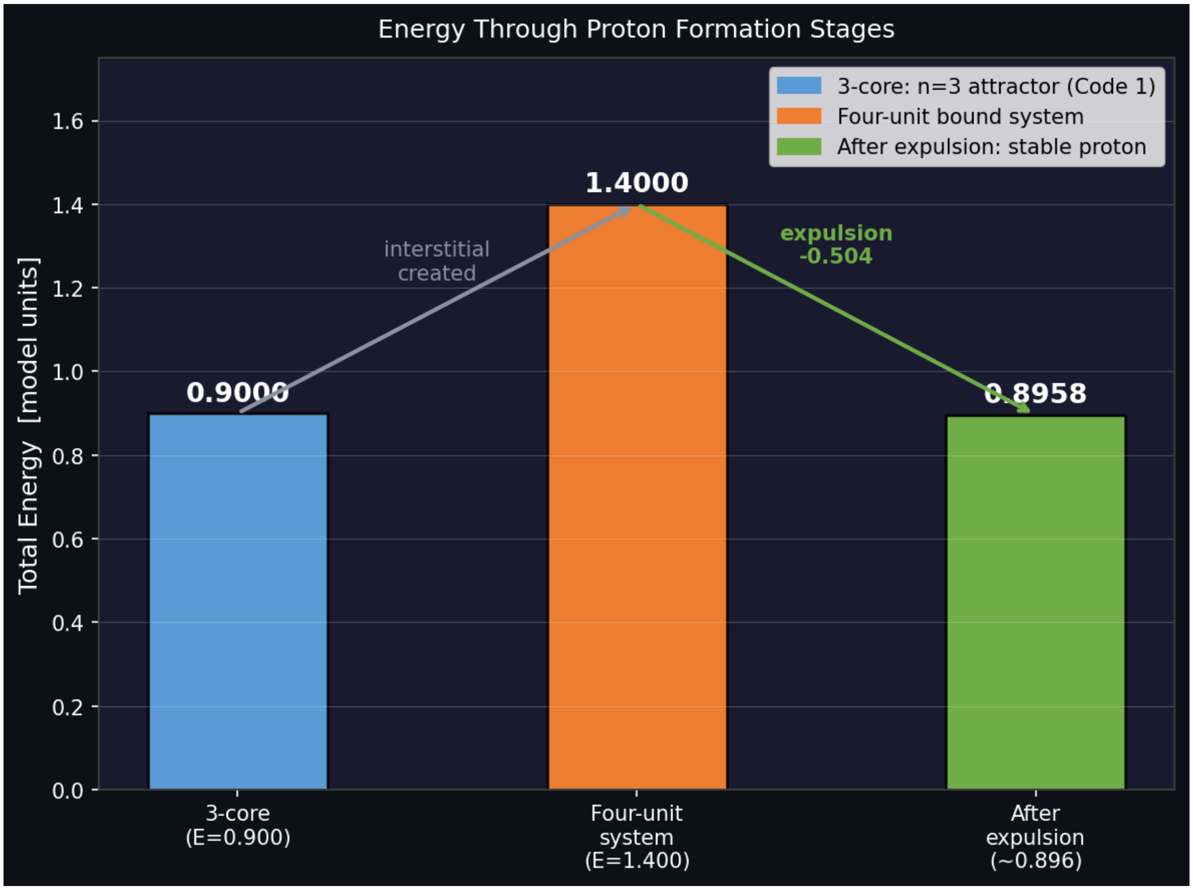

Figure D. Energy through the three stages of proton formation.

4. Three-Sphere Packing Geometry

Three substrate condensations of radius r_q in close-packed contact. The three centres form an equilateral triangle of side 2r_q. The outer radius of the assembly equals rp, the measured proton charge radius. This is the only measured input.

r_outer = r_q x (1 + 2/√(3)) = 2.1547 x r_q = rp

r_q = rp / (1 + 2/√(3)) = 0.8414 / 2.1547 = 0.3905 fm

Vgap / Vq = (2*√(3) - π) / (4*π/3) = 0.0770

Both results are universal geometric constants. No free parameters.

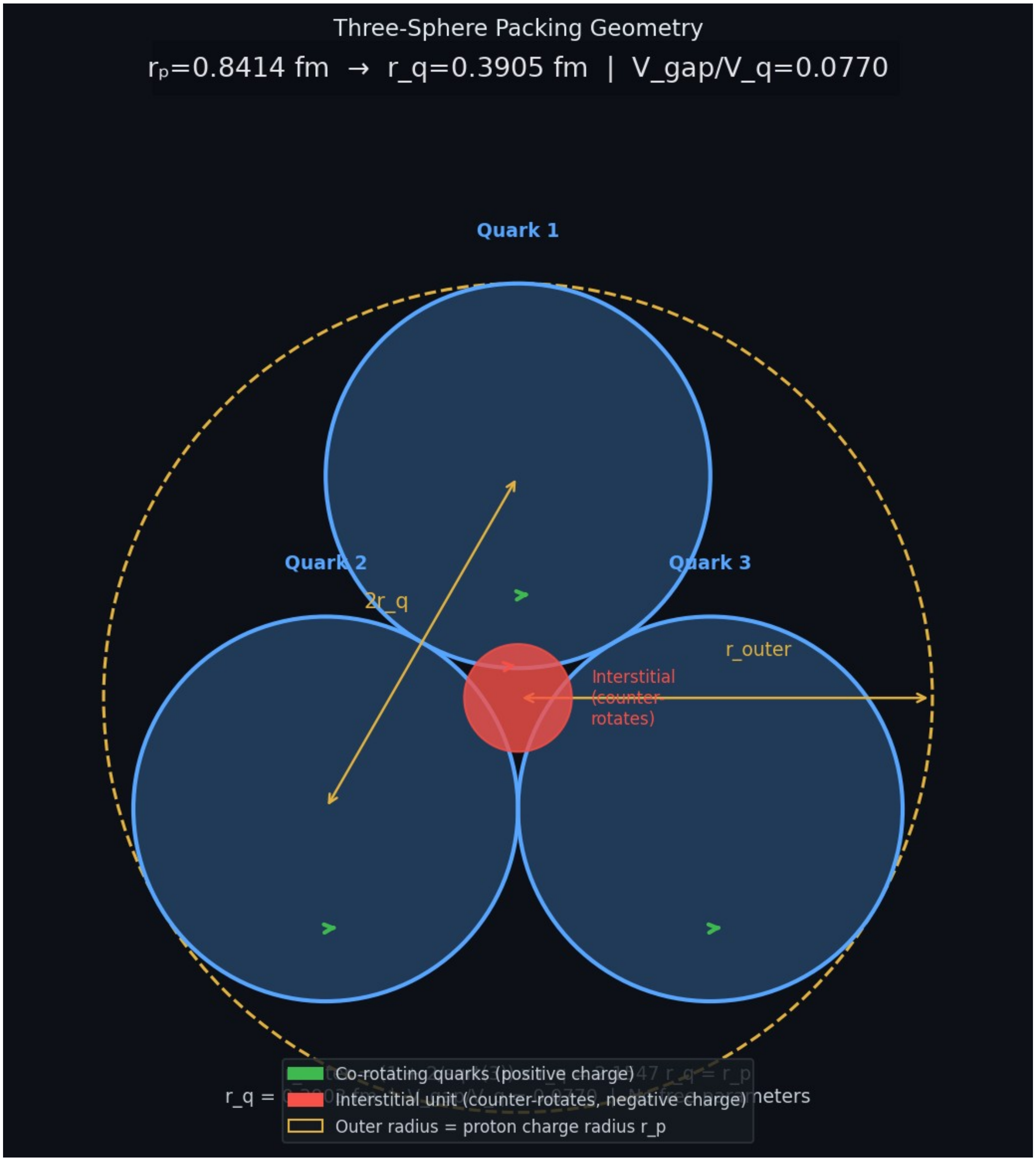

Figure E. Three-sphere packing geometry. Green arrows: co-rotating quarks. Red: interstitial unit (counter-rotates). Yellow dashed: outer radius = rp.

5. Why the Interstitial Unit Counter-Rotates

The counter-rotation is mechanically imparted, not assumed. When the interstitial substrate exits through the gap between any two quarks, it encounters two co-rotating surfaces - one on each side. Both quarks rotate in the same direction. Each imparts a tangential force in the opposite direction to the passing substrate. Together they impart a net counter-clockwise torque.

This is the gear analogy: a gear placed between two co-rotating gears of the same handedness always rotates in the opposite direction. The result is the same regardless of which gap the substrate exits from, because all three quarks rotate in the same direction.

Counter-rotation in BFUT is the definition of opposite charge. The negative charge of the expelled unit is therefore not assigned or assumed. It is mechanically imparted during expulsion by the same co-rotation that defines the quarks as positively charged.

6. Proton Energy with Interstitial Unit

When the detached unit has mass fraction μ relative to a core unit, the P16 functional is evaluated with s = [+1, +1, +1, -μ]. The geometric asymmetry term scales with μ because the geometric displacement is proportional to the actual mass of the detached unit:

$$
\begin{aligned}
E(\mu) = &-J \times \text{pairs\_sum}([1,1,1,-\mu]) \\
&+ \lambda \times (3-\mu)^2 \\
&+ (3-3)^2 + \alpha \times \mu \\
&+ D\_s \times (-1)
\end{aligned}
$$

At μ=1.0 (standard 3+1): E = 1.4000 model units (baseline confirmed)

Minimum: E = 0.8958 model units at μ = 0.083

Driving force for expulsion: -0.504 model units

μ	E(μ)	Reduction from 1.400	Note
1.000	1.4000	0.0000	Standard 3+1 baseline
0.500	1.0000	-0.4000	
0.230	0.9087	-0.4913	P19 upper bound
0.083	**0.8958**	**-0.5042**	**MINIMUM**
0.077	0.8959	-0.5041	P19 lower bound

The result is robust across the full physical range μ = 0.077 to 0.23. Proton stability does not depend on fine-tuning the interstitial mass fraction.

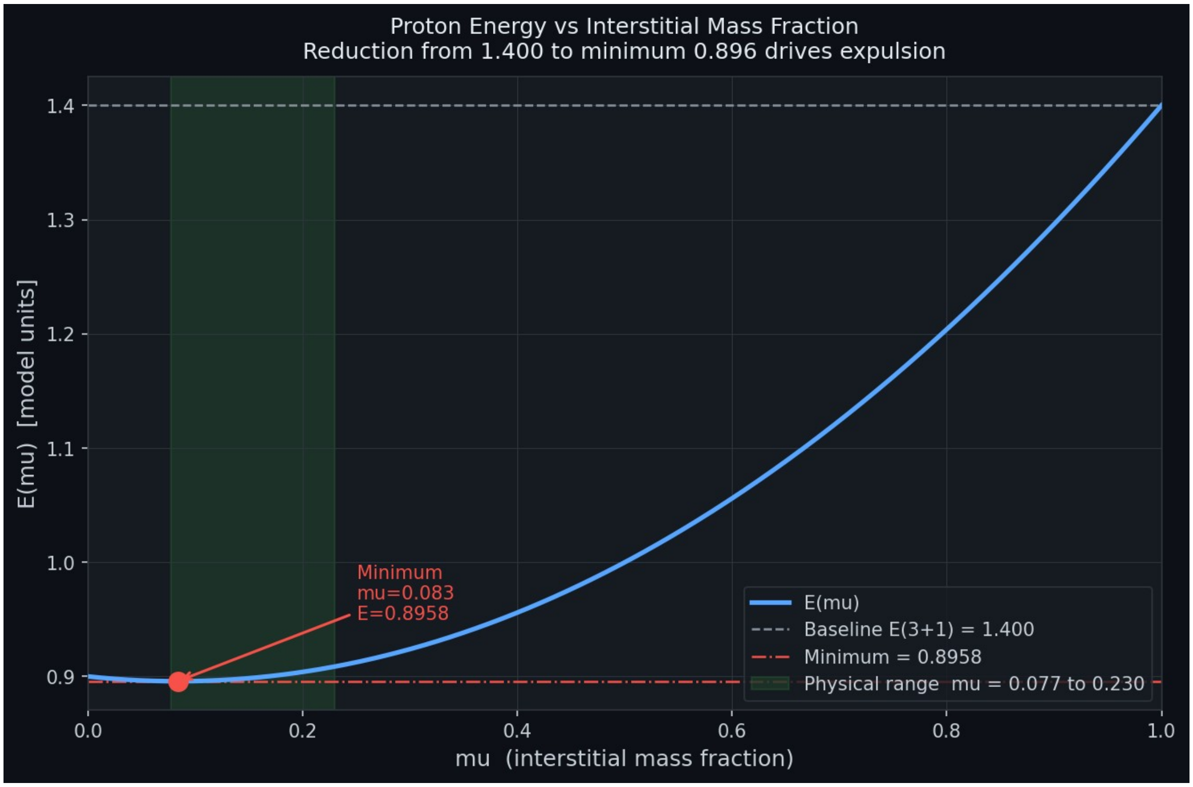

Figure F. E(μ) vs μ across the full range 0 to 1. Minimum at μ=0.083. Green band: physical range.

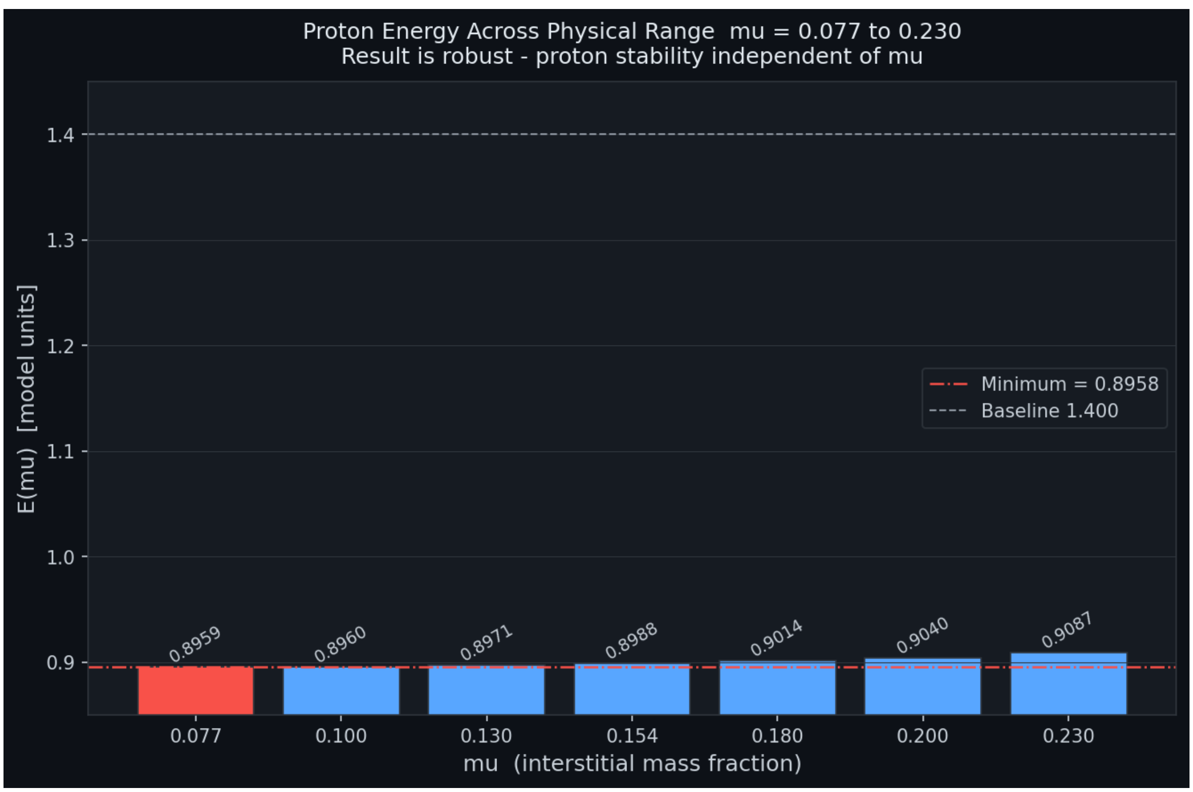

Figure G. Proton energy across the physical range μ=0.077 to 0.230. Result is robust.

7. The Connecting Identity

P19 Section 21.6 establishes an exact algebraic identity connecting the interstitial volume fraction, the electron mass, and the compression energy. E_unit cancels exactly - the identity is purely geometric:

Egap = E_unit x Vgap/Vq = 298.661 x 0.0770 = 22.999 MeV

m_e_vss = E_unit / (6 x π^4) = 298.661 / 584.45 = 0.511009 MeV

Egap / m_e_vss = 6 x π^4 x Vgap/Vq = 584.45 x 0.0770 = 45.00

Physical meaning: The expelled substrate dissipates 44/45 of the compression energy into the surrounding substrate during proton stabilisation. The remaining 1/45 is retained as the stable counter-rotating condensate whose mass is m_e_vss. The chain from Vgap to Egap to m_e_vss is one identity with E_unit as the common factor that cancels.

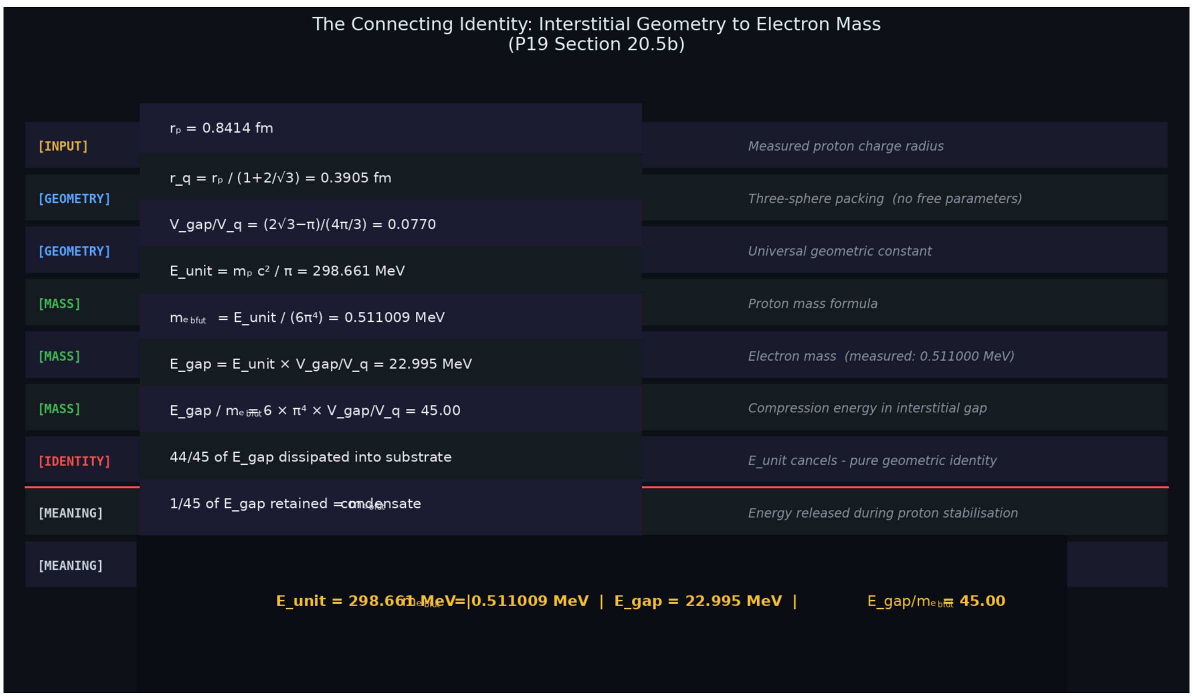

Figure H. The connecting identity chain from measured rp to m_e_vss. E_unit cancels at the IDENTITY step.

8. Modular Organisation: The Universal Structural Unit

For any n > 4 substrate units, multiple modular units are always energetically preferred over a single large condensate. The energy advantage grows with n. At n=24 the gap is 34.5 model units.

n	E single	k_opt	m x 1.400	Gap	Winner

4	**1.400**	**3**	**1.400**	**0.000**	**EQUAL**
5	2.100	3	1.750	+0.350	**MODULAR**
8	5.400	3	2.800	+2.600	**MODULAR**
12	11.100	4	4.200	+6.900	**MODULAR**
24	42.900	6	8.400	+34.500	**MODULAR**

The single condensate is free to choose any primary group size k. It chooses k=3 for n=4 to 8, then k=4, then k=5. It loses anyway. The modular unit is the universal preferred structural unit for matter at all scales.

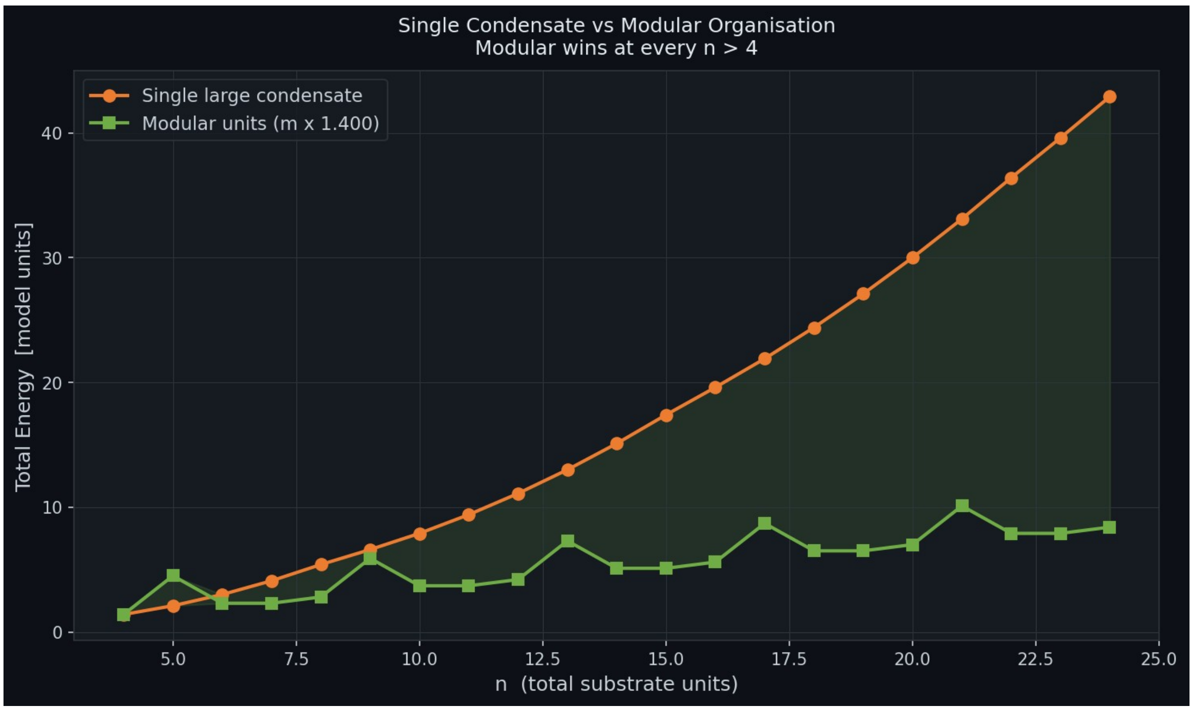

Figure I. Total energy: single condensate vs modular units for n=4 to 24.

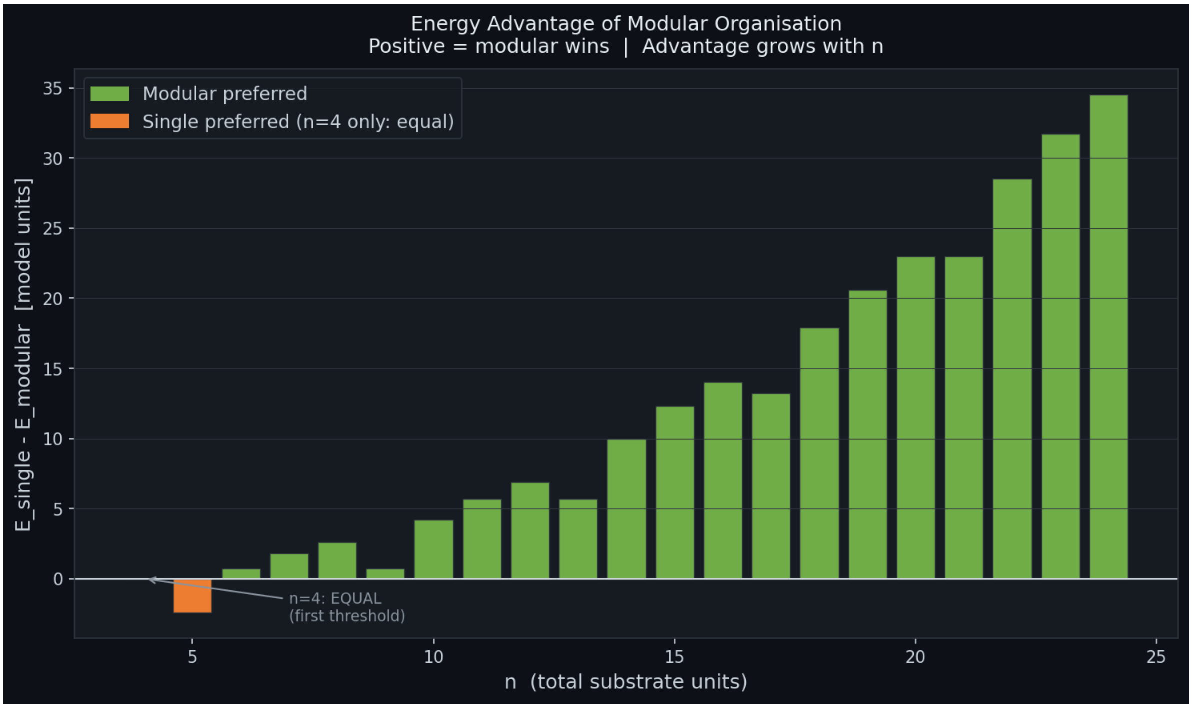

Figure J. Energy advantage of modular organisation. Positive = modular wins. Gap grows with n.

9. Robustness: Parameter Space Analysis

The 3+1 selection is not a fragile result at a single parameter point. Scanning λ and α across [0.2, 1.2] with J=1.0 fixed:

Scan	3+1 wins	Parameters varied
1D	**97.56%**	λ in [0.2, 1.2]
2D	**95.95%**	λ x α in $[0.2, 1.2]^2$
3D	**90.43%**	λ x α x D_s in $[0.2,1.2]^2$ x [0.5,2.5]

Comparison with the four-term baseline (without cos(3φ) term):

Scan	Four-term	Five-term	Improvement
1D	85.37%	**97.56%**	**+12.19%**
2D	83.82%	**95.95%**	**+12.13%**
3D	80.84%	**90.43%**	**+9.59%**

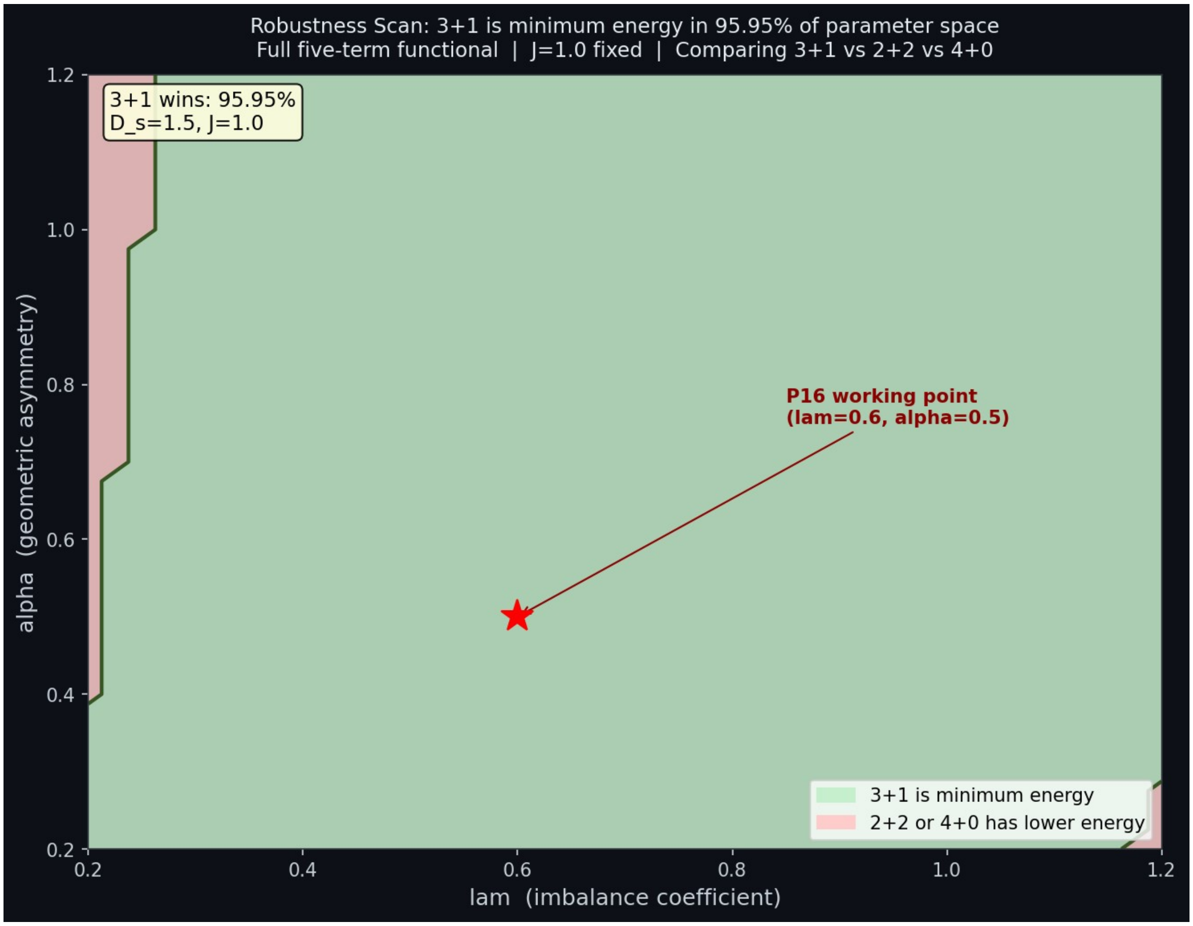

Figure K. Parameter space map. Green: 3+1 is minimum energy. Red: other configuration wins. P16 working point marked.

10. All Key Results at a Glance

Quantity	Value	Source
r_p	0.8414 fm	CODATA 2018 measurement
r_q	**0.3905 fm**	Three-sphere geometry
V_{gap} / V_q	**0.0770**	Universal geometric constant
E_unit = mp/π	**298.661 MeV**	Proton mass formula
m_e_vss = E_unit/(6*π⁴)	**0.511009 MeV**	Electron mass (measured: 0.510999)
E_{gap}/m_e_vss	**45.00**	Connecting identity - E_unit cancels
E(3+1) baseline	**1.4000 model units**	P16 functional, standard 3+1
E minimum (μ=0.083)	**0.8958 model units**	P16 functional, interstitial expelled
Driving force	**-0.504 model units**	Energetic basis for expulsion

2D robustness	**95.95%**	Five-term functional scan
Confinement F	**0.574 GeV/fm**	vs QCD 0.900 GeV/fm (36%)

Appendix F. Full P17 Force-Emergence Derivation

This appendix reproduces the P17 derivational chain needed for the present dark-matter identification so the gravitational, strong, electromagnetic, and weak substrate mechanisms are available within this paper.

F.1 Gravity from Spaticle-field deformation

The Spaticle field is a physical matter substrate with equilibrium density ρ_s. A matter condensation changes the local substrate configuration. The resulting deformation is gravitationally active because the substrate carries density and stress-energy.

$$G_{\mu\nu} = (8\pi G/c^4)[T_{\mu\nu}^{(m)} + T_{\mu\nu}^{(s)}]$$

In the weak-field description, the substrate contribution can be written as a gradient-sourced density:

$$\rho_\nabla = |\nabla\Psi|^2/c^2$$

$$\nabla^2\Psi = 4\pi G[\rho b + \rho_s + \rho_\nabla]$$

The P17 field equation and the P18 carrier equation describe complementary levels of the same substrate dynamics. P17 specifies how the substrate configuration contributes to gravitational source structure; P18 specifies the finite-response carrier dynamics.

F.2 Strong interaction from condensation mechanics

$$E_{total}(d) = 2E_{cond} + E_{overlap}(d) + E_{compression}(d) + E_{reconfiguration}(d)$$

$$E_{overlap}(d) = -A_s \exp(-d/L_{rlx})$$

$$E_{compression}(d) = B_s(r_p/d)^{12}$$

$$E_{reconfiguration}(d) = C_s\, d$$

The overlap term produces attraction between co-rotating condensations, the compression term produces hard-core repulsion, and the linear reconfiguration term produces confinement. P17 gives $C_s = F_{conf}$ = 0.574 GeV/fm from the condensation energy density, providing the substrate origin of the confinement scale.

F.3 Electromagnetism from rotational asymmetry

The 3+e bifurcation established in P16 creates persistent internal circulation asymmetry. The surrounding substrate responds to this directional asymmetry, producing the electromagnetic field.

$$(1/c^2)\, \partial^2 A/\partial t^2 - \nabla^2 A + \beta A + \kappa_{EM}(A\cdot A)A = J^{(rot)}$$

For the electromagnetic mode $\beta(EM)=0$. The photon is therefore a massless propagating substrate excitation. The source term $J^{(rot)}$ changes sign with the circulation orientation of the charged condensation.

F.4 Weak interaction from topology reconfiguration

The weak interaction is a substrate-topology transformation mechanism. W and Z excitations carry the reorganisation energy needed to transform one internal condensation state into another.

$$L(W) = \hbar\_vss/[m(W)c]$$
$$L(Z) = \hbar\_vss/[m(Z)c]$$
$$\chi = \mathrm{sign}(\Omega e\cdot\hat{p}) = -1$$
The counter-rotation generated by the P16 3+e geometry supplies the weak-sector chirality structure. The BFUT mixing quantity is obtained only after the independent W and Z resonance masses, from their squared mass ratio.

Appendix G. Full P18 Gravitation, DDR, and DME Derivation

This appendix gives the complete P18 derivational chain used by P25: the substrate density, covariant carrier equation, finite deformation domain, DME equation, and observational applications.

G.1 Density-derived carrier scale

$$\mu_s^2 = 3G\rho_s/c^2$$
$$\mu_s = 4.03358955 \times 10^{-27}\ \mathrm{m}^{-1}$$
$$Ls = 1/\mu_s = 2.47918135 \times 10^{26}\ \mathrm{m} = 26.205\ \mathrm{Gly}$$
$$a_s = c^2\mu_s/3 = c\sqrt{(G\rho_s/3)} = 1.20840317 \times 10^{-10}\ \mathrm{m\ s^{-2}}$$

G.2 Fully covariant carrier equation

$$g^{\mu\nu}\nabla\_\mu\nabla\_\nu(\delta\Psi) - \mu_s^2\delta\Psi = \kappa_s\nabla^2\Psi\mathrm{matter}, \quad \kappa_s = 1/c^2$$
The equilibrium solution is $\delta\Psi = 0$, with the carrier response governed by the density-derived scale μ_s. The local transient relaxation length is $L\_rlx = c\tau\_c$.

G.3 Finite deformation-domain radius

$$Rd = [3M/(8\pi\rho_s)]^{1/3}$$
$$Meff = M(1 + vrot^2/c^2)$$
$$R\_eff = Rd(1 + vrot^2/c^2)^{1/3}$$
The base domain radius is fixed by source mass and the intrinsic substrate density. Rotational enhancement changes the domain boundary through Meff. The DME rotational support itself is supplied by the organised entrainment law below.

G.4 DME equation

$$vb^2(R) = vgas|vgas| + Yvdisk^2 + Yvbulge^2, \quad Y = 0.5$$
$$v^2(R) = vb^2(R)[1 + a_sR/vb^2(R)]^{1/2}$$
$$g\_DME(R) = g\_b(R)[1 + a_s/g\_b(R)]^{1/2}$$
$$M\_extra(<R) = M\_b(R)\{[1 + a_sR^2/(GM\_b(R))]^{1/2} - 1\}$$
The theoretical acceleration scale a_s is computed once from ρ_s, G, and c and is held fixed across the full sample.

G.5 SPARC validation

P18 applies the DME equation to all 175 SPARC galaxies using the published baryonic rotation components and Y=0.5. The reported results are 92.0% shape agreement, 98.8% flat classification, 14.3% non-flat classification, and a median outer relative residual of 0.096.

G.6 KiDS-1000 weak lensing

$$v_b^2(R) = GM_{gal}/R$$
$$v^2(R) = v_b^2(R)[1 + a_s R/v_b^2(R)]^{1/2}$$
$$v^4 = GM_{gal}\, a_s \quad \text{(deep organised regime)}$$

The same a_s is used for the four KiDS-1000 stacked lensing bins. The reported DME result is $\chi^2/N = 9.78$ for the 60 measurements.

Appendix H. Current P19 Particle and Electroweak Derivation

This appendix records the P19 derivation chain: independent Z and W resonances from the P16 condensation structure, the mixing quantity as their mass-ratio output, and the H-class radial resonance of the single Spaticle field.

H.1 Particle-sector scale inherited from P16

$$E(R) = A/R^2 + BR^2 + CR + D/R$$
$$A = 0.5,\ B = 0.56308,\ C = -1/3,\ D = 1$$
$$R_0 = 1.27348221$$
$$\ell\_model = rp/R_0 = 6.607081 \times 10^{-16}\ \text{m}$$
$$\hbar\_vss = mpc\ell\_model/\pi = 1.0545769 \times 10^{-34}\ \text{J s}$$
$$m\_e\_vss = mp/(6\pi^5) = 9.1095552 \times 10^{-31}\ \text{kg}$$
$$\alpha\_vss = e^2/(4\pi\varepsilon_0\hbar\_vssc) = 0.007297318 = 1/137.036655$$
$$m^*\_vss = m\_e\_vss/\alpha\_vss = 1.2483430 \times 10^{-28}\ \text{kg}$$
$$r_e\_vss = \alpha\_vss\hbar\_vss/(m\_e\_vssc) = 2.8178873 \times 10^{-15}\ \text{m}$$
$$u\_g = G(m\_*)^2/(8\pi r_e^4) = 6.5635567 \times 10^{-10}\ \text{J m}^{-3}$$
$$\rho_s = ug/c^2 = 7.3 \times 10^{-27}\ \text{kg m}^{-3}$$

H.2 Fine-structure constant

$$\alpha\_vss = e^2/(4\pi\varepsilon_0\hbar\_vssc)$$
$$\hbar\_vss = mpc\ rp/(\pi R_0)$$
$$\alpha\_vss = e^2R_0/(4\varepsilon_0 mpc^2 rp) = 1/137.037$$

The condensation-derived R_0 therefore supplies the geometric scale entering α_vss. The result agrees with the measured value to 0.00048%.

H.3 Strong coupling

$$\alpha s\_vss = B\ R_0^4/(8\pi A)$$
$$\alpha s\_vss = 0.56308(1.27348221)^4/[8\pi(0.5)] = 0.11785$$

Running to the m_Z scale gives αs_vss = 0.1178, with the P19 comparison value differing by 0.043%.

H.4 Electroweak mixing

The P19 mixing quantity is derived only after the independent W and Z resonance masses: $\sin^2\theta\_W\_vss = 1 - (m\_W\_vss/m\_Z\_vss)^2 = 1 - 256^2/(9\pi^8) = 0.23257$.

The mixing quantity is an output of the two independently derived resonance masses and is not used as a parent input to either mass.

H.5 W and Z masses

The charged and neutral resonance masses are independent outputs: m_W_vss = 256M = (256/3)mp = 80.066 GeV/c^2 and m_Z_vss = π^4mp = 91.396 GeV/c^2; neither is derived from the mixing angle.

$$m\_W\_vss = 80.066\ \mathrm{GeV}/c^2$$

The charged and neutral resonance masses are independent outputs: $m\_W\_vss = 256M = (256/3)mp = 80.066\ \mathrm{GeV}/c^2$ and $m\_Z\_vss = \pi^4 mp = 91.396\ \mathrm{GeV}/c^2$; neither is derived from the mixing angle.

The electroweak W and Z masses are obtained from the P16/P19 condensation structure and proton mass anchor.

H.6 Higgs mass

The H-class resonance follows from the P16/P19 radial condensation invariant: $\lambda\_H\_vss = 2AR_0/\pi^2 = R_0/\pi^2$, $v\_vss = 6E\_unit/\alpha\_vss$, and $m\_H\_vss = v\_vss\sqrt{2\lambda\_H\_vss} = 124.75\ \mathrm{GeV}/c^2$.

The P19 radial-resonance chain gives $m\_H\_vss = 124.75\ \mathrm{GeV}/c^2$.

H.7 Substrate energy density

$$u\_vac = \rho_s c^2 = 6.5635567 \times 10^{-10}\ \mathrm{J\ m^{-3}}$$

This is the equilibrium rest-energy density of the physical Spaticle substrate. The equality follows directly from mass-energy equivalence once ρ_s has been independently fixed by the particle-sector chain.

Appendix I. Self-Contained Dark-Matter Identification Chain

The dark-matter identification follows by joining the four derivational papers without introducing a new theoretical ingredient.

P16: ρ_s → condensation geometry → stable 3+e matter → ħ_vss, m_e_vss, α_vss

P17: 3+e substrate organisation → gravity + strong + electromagnetic + weak interactions

P18: ρ_s → μ_s → F1-cov → Rd → a_s → DME → galaxy rotation + weak lensing

P19: P16 condensation geometry + proton anchors → α_vss, αs_vss, m_Z_vss, m_W_vss, sin²θ_W_vss, λ_H_vss, v_vss, m_H_vss.

The same physical substrate is present in both particle and gravitational sectors, but the numerical provenance differs by sector: ρ_s enters the gravitational DME chain, while the W, Z, mixing quantity, and H-class resonance follow from P16/P19 condensation invariants and proton-scale anchors.

The identification is consequently a physical statement about the referent of the observed gravitational component: dark matter is the Spaticle field. The field is non-electromagnetic, gravitationally active, spatially extended through its deformation domains, and capable of being organised by rotating matter. The DME equation provides the quantitative connection to the observed extra gravitational support.

$$a_s = c\sqrt{G\rho_s/3} = 1.20840317 \times 10^{-10}\ \mathrm{m\ s^{-2}}$$

$$v^2(R) = vb^2(R)[1 + a_s R/vb^2(R)]^{1/2}$$

The identification is supported simultaneously by particle-sector calibration, electroweak mass relations, hydrogen stability, finite gravitational domains, the SPARC rotation-curve sample, and KiDS-1000 weak lensing, all using the same adopted substrate density.

References

[1] Sharma, V. S. (2026). The Origin of Matter, Antimatter, and Fundamental Forces: How Protons, Electrons, and Hydrogen Formed Fundamental Forces. BFUT P16. Zenodo. DOI: 10.5281/zenodo.19908215

[2] Sharma, V. S. (2026). The Emergence of Forces and Fundamental Senses: How the Spaticle Field Gave Rise to Gravity and All Other Forces. BFUT P17. Zenodo. DOI: 10.5281/zenodo.19976408

[3] Sharma, V. S. (2026). Beyond General Relativity: A Unified Gravitation Equation Across Quantum, Classical, Galactic, and Rapid-Transition Regimes. BFUT P18. Zenodo. DOI: 10.5281/zenodo.20145506

[4] Sharma, V. S. (2026). Unification of Particle Physics: Deriving Fine Structure and Coupling Constants, W, Z, and Higgs Boson Masses, Redefining and Unifying Gravity and Time. BFUT P19. Zenodo. DOI: 10.5281/zenodo.20145567
[5] Lelli, F., McGaugh, S. S., & Schombert, J. M. (2016). SPARC: Mass Models for 175 Disk Galaxies with Spitzer Photometry and Accurate Rotation Curves. The Astronomical Journal, 152(6), 157.
[6] Brouwer, M. M., et al. (2021). KiDS-1000 weak gravitational lensing and the radial acceleration relation. Astronomy & Astrophysics.
[7] Clowe, D., et al. (2006). A Direct Empirical Proof of the Existence of Dark Matter. The Astrophysical Journal Letters, 648(2), L109-L113.
[8] Zyla, P. A., et al. (Particle Data Group). (2020). Review of Particle Physics. Progress of Theoretical and Experimental Physics, 2020, 083C01.
[9] ATLAS Collaboration: Aad, G., et al. (2012). Observation of a new boson at a mass of 125 GeV with the ATLAS detector at the LHC. Physics Letters B, 716(1), 1-29.
[10] CMS Collaboration: Chatrchyan, S., et al. (2012). Observation of a new boson at a mass of 125 GeV with the CMS experiment at the LHC. Physics Letters B, 716(1), 30-61.
[11] Sharma, V. S. (2026). The Spaticle Field as the Unified Substrate of Physical Reality. BFUT P14. Zenodo. DOI: 10.5281/zenodo.19394064